Applied Energy 210 (2018) 28–43

Contents lists available at ScienceDirect

Applied Energy

journal homepage: www.elsevier.com/locate/apenergy

Effect of organic type and moisture on CO_2/CH_4 competitive adsorption in kerogen with implications for CO_2 sequestration and enhanced CH_4 recovery

Liang Huang[a,b,*], Zhengfu Ning[a,b], Qing Wang[a,b], Wentong Zhang[a,b], Zhilin Cheng[a,b], Xiaojun Wu[a,b], Huibo Qin[c]

[a] State Key Laboratory of Petroleum Resources and Prospecting, China University of Petroleum (Beijing), Beijing 102249, PR China
[b] Department of Petroleum Engineering, China University of Petroleum (Beijing), Beijing 102249, PR China
[c] State Key Laboratory of Heavy Oil Processing, China University of Petroleum (Beijing), Beijing 102249, PR China

HIGHLIGHTS

- Realistic kerogen models are utilized to quantify CO_2/CH_4 competitive adsorption.
- Effect mechanisms of organic type and moisture on gas adsorption are elaborated.
- Dynamic distribution characteristic of moisture in kerogen models is revealed.
- Kerogen IIIA is the optimized organic type for CS-EGR.
- Moisture can potentially boost the displacement of CH_4 by CO_2.

ARTICLE INFO

Keywords:
CO_2 sequestration
Enhanced gas recovery
Competitive adsorption
Organic type
Moisture
Microscopic mechanism

ABSTRACT

Although research attentions for CO_2 injection in gas-bearing reservoirs have been drawn to CO_2 sequestration with enhanced gas recovery (CS-EGR), the microscopic competitive adsorption mechanism of methane (CH_4) and carbon dioxide (CO_2) considering the effect of organic type and moisture remains to be determined. In this work, we focus on the competitive adsorption behaviors of CH_4 and CO_2 on dry and moist realistic kerogen models of different organic types by performing combined molecular dynamics (MD) and grand canonical Monte Carlo (GCMC) simulations. The effects of organic type and moisture content on kerogen pore structures, moisture distribution and interaction between CH_4/CO_2 and kerogen surfaces are discussed in details. Simulation results show that CO_2/CH_4 adsorption capacity and adsorption selectivity are in the order of kerogen IA < IIA < IIIA, consistent with the sequence of enterable pore volume fraction (IA, 9.38%; IIA, 13.59%; IIIA, 28.88%). H_2O molecules are preferentially adsorbed on the sulfur- and oxygen-containing groups at low moisture, and then migrate and aggregate into clusters in the middle of enterable pores at high moisture. The CO_2/CH_4 adsorption capacity decreases with increasing moisture content, while the CO_2/CH_4 adsorption selectivity, specific adsorption energy and CO_2 isosteric heat decrease at the beginning, and then increase with the moisture content. Moisture has a bigger effect on the adsorption of CO_2 than that of CH_4. This study indicates that kerogen IIIA is the optimized organic type for CS-EGS due to its large and stable CO_2 storage capacity. Despite its negative effect on gas adsorption capacity, moisture can potentially boost the displacement of CH_4 by CO_2 at certain moisture conditions. Results of this study lay the foundation for future optimization design of CS-EGR projects with application to coal and shale systems.

1. Introduction

As important substitutes for conventional hydrocarbon resources, coalbed methane (CBM) and shale gas have attracted global focus because of their considerable resource abundance, high utilization efficiency and environmental friendliness [1–5]. However, it should be noted that tight reservoir characteristics and complex gas transport mechanisms, as well as depleted development regime have led to a low recovery of CBM and shale gas reservoirs [6–8]. With the increasing demand for clean fossil fuels, interest in enhanced gas recovery in these unconventional reservoirs has grown sharply. Injection of CO_2 into gas-bearing layers has been accepted as a viable strategy for underground

* Corresponding author at: State Key Laboratory of Petroleum Resources and Prospecting, China University of Petroleum (Beijing), Beijing 102249, PR China.
E-mail address: huangliang19911015@163.com (L. Huang).

http://dx.doi.org/10.1016/j.apenergy.2017.10.122
Received 31 July 2017; Received in revised form 26 October 2017; Accepted 30 October 2017
Available online 02 November 2017

Nomenclature

Symbols	physical (Units)
E_a	adsorption energy (kJ/mol)
E_{AB}	energy of the mixtures of A and B (kJ/mol)
E_A	energy of isolated component A (kJ/mol)
E_B	energy of isolated component B (kJ/mol)
N	number of adsorbed molecules (dimensionless)
n	gas adsorption amount (mmol/g)
n_a	absolute adsorption amount (mmol/g)
n_e	excess adsorption amount (mmol/g)
p	pressure (kPa)
Q_{st}	isosteric adsorption heat (kJ/mol)
R	universal gas constant (kJ/(mol·K))
S_{CO_2/CH_4}	CO_2/CH_4 adsorption selectivity (dimensionless)
T	temperature (K)
x_i	mole fraction of component i in the adsorption phase (dimensionless)
y_i	mole fraction of component i in the bulk phase (dimensionless)
ρ	gas density (mmol/cm^3)
υ	free pore volume (cm^3/g)

CO_2 sequestration and enhanced gas recovery in CBM reservoirs, which can reduce the CO_2 emission and mitigate the global warming [9–12]. This technique has recently been considered as one potential strategy for CS-EGR in shale gas reservoirs [13,14]. A better understanding of CO_2/CH_4 competitive adsorption behaviors in coal and shale systems can help provide applicable guidelines for the design of the CS-EGR technique.

Coal is one kind of organic material, in which adsorbed gas is the dominant occurrence form. By comparison, shale gas is composed of free gas in fractures and big pores, absorbed gas in liquid phase and adsorbed gas in organic matter and clay minerals [15]. Of the three forms, adsorbed gas takes up a large proportion of the total share, which, for example, can account for 60–85% in the Lewis organic-rich shale [16]. Most of the adsorbed gas is stored in the nanopores of organic matter due to their large specific surface areas and strong adsorption potential [17,18]. Wang et al. [19] reported that almost half of the total hydrocarbons are adsorbed in the organic matter of gas shale. Clay minerals have less contribution to the adsorbed gas content due to their hydrophilic nature, which greatly reduces the gas adsorption capacity [20,21]. As a result, gas adsorption behaviors in organic matter can reflect the main adsorption characteristics of coal and organic-rich gas shale. According to the classification of Tissot and coworkers [22], organic matter can be sorted as three types, namely type I, type II and type III. The organic type is closely relevant to the compositional parameters, surface functional groups, molecular structure and micropore volumes, which greatly influence the gas adsorption behaviors [23]. The competitive adsorption performances of CO_2 over CH_4 in different organic types can help evaluate the potential of CS-EGR technique in different unconventional gas reservoirs.

Another key parameter associated with gas adsorption is the moisture of organic matter. Organic matter in coal and gas shale is traditionally deemed as hydrophobic [24]. But recent experimental and simulation work concluded that organic matter is actually mixed-wet, wherein the carbon skeleton is hydrophobic, while the carboxylic and hydroxylic functional groups are hydrophilic [25,26]. Organic matter in coal and shale is originally moisture equilibrated under reservoir conditions [27]. Moreover, the process of hydraulic fracturing increases the reservoir moisture contents by injecting a large amount of water-based fluids. Moisture can fill micropore throats and occupy gas sorption sites, leading to a rapid reduction of gas adsorption capacity [28]. In spite of these negative impacts, there are some beneficial characteristics of moisture under reservoir conditions. In addition to the advantage of proppant-carrying capacity, moisture can keep the concentration of brine to avoid the precipitation of minerals that may block small throats [13]. The effect of moisture on gas adsorption is closely correlated with the microscopic distribution of moisture in the pore system. Unfortunately, there are only few reported papers focusing on this topic [29,30]. The dynamic distribution of moisture in organic matter and its effect on CO_2/CH_4 competitive adsorption can not only provide a better understanding of the storage of initial water and the fate of residual treatment liquid, but also provide applicable guidelines for the evaluation of original gas reserves, the design of fracturing process and the optimization of CS-EGR technique. Accordingly, the influence mechanisms of organic types and moisture on CO_2/CH_4 competitive adsorption behaviors in organic matter are of fundamental significance to help improve the efficiency of CS-EGR technique with application to coal and shale systems.

Although the technique of CO_2 injection into shale and coal systems has not yet been commercialized, extensive investigations have been conducted on this subject. To date, the studies of CS-EGR performance have been widely carried out through the numerical simulations [8,31–35], experimental measurements [36–43], and molecular simulations [44–53], aiming to validate the feasibility and further provide applicable guidelines for the CS-EGR projects. Numerical simulation can study the performance of CS-EGR project in field scale, which is especially beneficial for evaluating the CO_2 injection scenario [8] and investigating the influence of reservoir heterogeneity and well placement on CS-EGR performance [31]. Yu et al. [32] and Jiang et al. [33] conducted numerous sensitivity studies of CS-EGR performance in shale reservoirs. Godec et al. [34] performed a numerical study on the CS-EGR performance in Marcellus Shale. Liu et al. [35] conducted a reservoir simulation of CO_2 injection in Devonian and New Albany shale gas reservoir. Results of all these numerical simulations indicated that injecting CO_2 into depleted shale gas reservoirs for CO_2 storage with enhanced gas recovery is technically feasible. However, it should be noted that numerical study generally relies on simplified reservoir model and assumptions, making it difficult to capture complex fluid-fluid and fluid-wall interactions considering the effect of organic type and kerogen moisture content.

Compared with numerical simulation, experimental measurement at laboratory scale is the more direct method to represent the realistic interplay of CO_2 with subsurface fluids and adsorbents. Many experimental work has been focused on the subject of CS-EGR. Some work has concluded the preferential adsorption of CO_2 over CH_4, indicating that CO_2 storage can be an effective method for enhancing gas recovery in shale reservoirs [36–40]. Nevertheless, there are many experimental studies indicating a higher adsorption capacity for CH_4 over CO_2 at low pressure conditions [41,42]. Therefore, the feasibility of CS-EGR remains to be further verified for experimental investigations. It is difficult to understand the microbehaviors of CH_4 and CO_2 in realistic nanoporous adsorbents through experimental measurement due to the heterogeneous nature of experimental samples [43]. Also, many shale reservoirs are originally at extremely high temperature and pressure conditions, which are challenging for the present experimental apparatuses to withstand.

By contrast, molecular simulation is a powerful tool to gain insights into the microbehaviors of gases in complex systems at microscopic level accurately and intuitively, complementary to the experimental measurement [44]. Concerning the CS-EGR technique, many attempts have been conducted to investigate the CO_2/CH_4 competitive adsorption behaviors in nanopores of organic matter using molecular simulation techniques [44–53]. However, most of these simulation studies are performed on simplified adsorbents like graphene slits, nanoporous carbons and carbon nanotubes [45–51]. For example, Kazemi et al. [45]

and Kurniawan et al. [46] investigated the CO_2/CH_4 competitive adsorption behaviors in graphene slits. Yuan et al. [47] studied the microbehaviors of CO_2 displacing confined CH_4 in carbon nanotubes. Brochard et al. [48] examined the competitive adsorption behaviors of CO_2/CH_4 mixtures in a carbon-based coal model, while Wang et al. [49] studied the CO_2/CH_4 competitive adsorption behaviors in a carbon-based model representative of organic matter in shale. Meanwhile, some investigations have been performed on simplified carbon-based models with surface heterogeneity. Lu et al. [50] explored the influence of edge-functionalization on CO_2/CH_4 competitive adsorption in nanoporous carbons. Liu et al. [51] performed the competitive adsorption of CO_2/CH_4 binary mixtures in carbon-based coal models with heterogeneous surfaces. They presented the influence of moisture content, but the detailed effect mechanisms of moisture content were not included in their study. Although these studies performed on simplified models can provide us with some guidelines about the CO_2/CH_4 competitive adsorption behaviors, the guidelines are limited, because these simplified models fail to capture the physically and chemically heterogeneous nature of authentic organic matter in coal and shale systems. Recently, some researches have been conducted to investigate the CO_2/CH_4 competitive adsorption on realistic organic matter models, and sensitivity analysis on various parameters have been performed to provide applicable guidelines for improving the efficiency of CS-EGR project with application to shale and coal systems. Zhang et al. [44] studied the CO_2/CH_4 competitive adsorption behaviors in nanopores of a realistic bituminous coal model. They discussed the effect of CO_2 injection depths and gas compositions on CO_2/CH_4 adsorption selectivity, suggesting that shallow reservoir depths and low CO_2 compositions are optimized conditions for the CS-EGR project. Sun et al. [52] investigated the CO_2/CH_4 competitive adsorption behaviors and the efficiency of CO_2 displacing residual CH_4. They concluded that high reservoir pressure is beneficial for CO_2 sequestration and CH_4 displacement. Unfortunately, the influence of organic type and moisture content were not discussed in their work. Huang et al. [53] simulated the competitive adsorption behaviors of CO_2/CH_4 mixtures in realistic kerogen models with different maturities and moisture contents. Although the effect of moisture content was analyzed, the dynamic distribution characteristics of moisture were not explored.

In spite of previous researches, the competitive adsorption process of injected CO_2 with subsurface CH_4 in shale and coal reservoirs in terms of the CS-EGR technique is still in a preliminary stage. So far, there are only a very limited number of studies focused on the CO_2/CH_4 competitive adsorption in realistic organic matter models. Previous studies have considered only the effect of moisture content on the CO_2/CH_4 competitive adsorption behaviors, the dynamic distribution characteristics of moisture and the effect of organic type have not yet been explored. To our best knowledge, the detailed influence mechanisms of organic type and moisture content on the CO_2/CH_4 competitive adsorption behaviors in realistic kerogen remain undetermined, and their implications for improving the CS-EGR efficiency need to be explored.

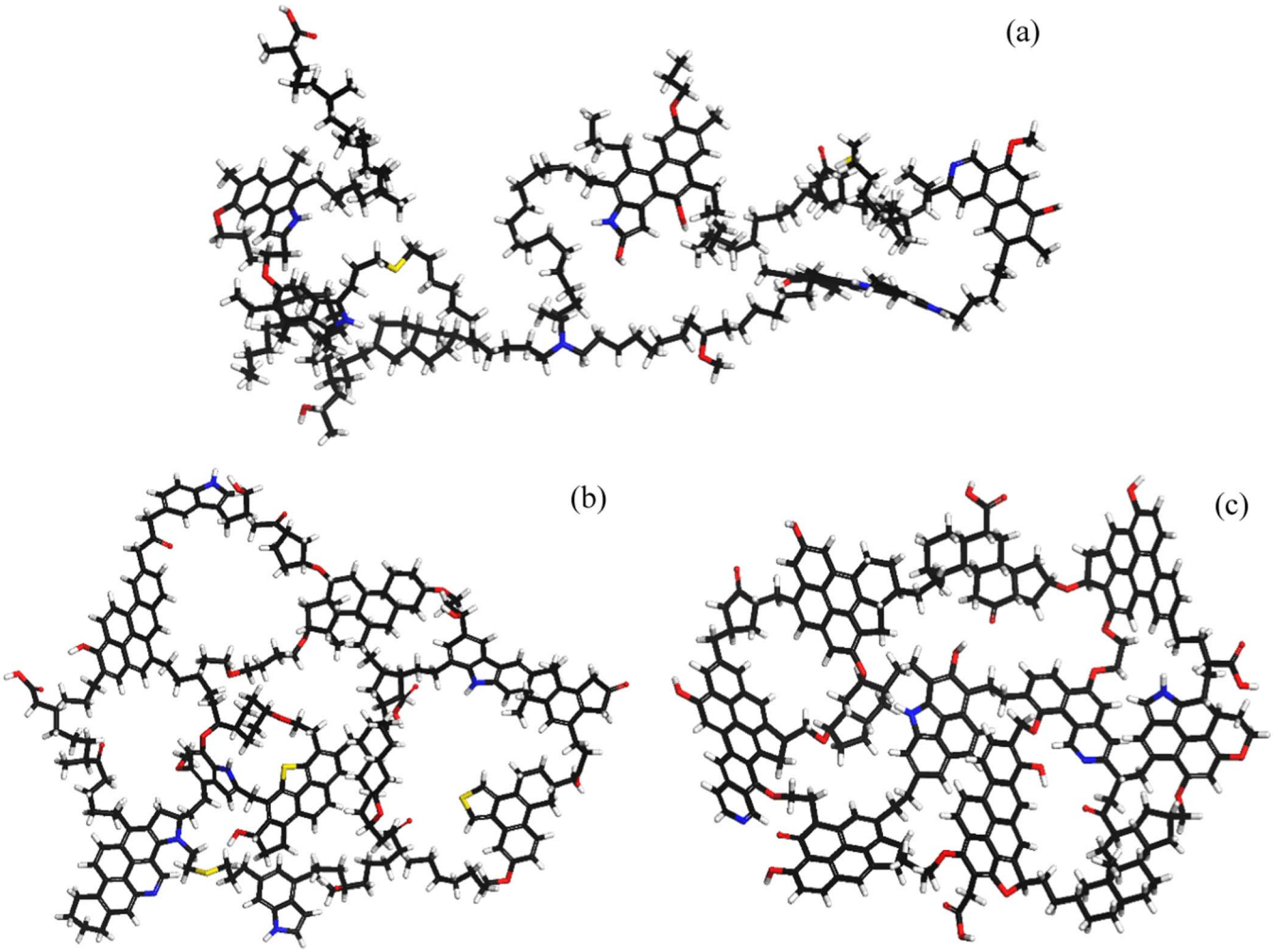

Fig. 1. Kerogen structure units used in this study established by Ungerer et al. [23] based on experimental data documented by Kelemen and coworkers [54]. (a) Kerogen type IA with a chemical formula of $C_{251}H_{385}O_{13}N_7S_3$; (b) kerogen type IIA with a chemical formula of $C_{252}H_{294}O_{24}N_6S_3$; (c) kerogen type IIIA with a chemical formula of $C_{233}H_{204}O_{27}N_4$. Atom representations: black for carbon atoms, grey for hydrogen atoms, red for oxygen atoms, yellow for sulfur atoms, and blue for nitrogen atoms.

The objective of our work is to gain insights into this topic.

In this study, realistic kerogen models of different organic types with physically and chemically heterogeneous nature were developed using the MD method. These dry kerogen models were firstly validated by comparing the atomic compositions, functional groups, physical densities and porosities, and CH_4 excess adsorption isotherms with experimental data, and then utilized to construct moist kerogen models with various moisture contents (0.6, 1.2, 1.8, 2.4 wt%). The CO_2/CH_4 competitive adsorption behaviors in these kerogen models considering the effect of organic type and moisture content were investigated through GCMC simulations. The effects of both physical pore structure and surface chemically heterogeneity associated with organic type on CO_2/CH_4 adsorption capacity, adsorption selectivity and isosteric heat were discussed. The affinity between CH_4/CO_2 and different functional groups in kerogen models were analyzed by computing the radial distribution function (RDF). To explore the dynamic distribution of moisture at molecular level, we compared the pore size distributions and pore volume distributions of kerogen models under different moisture contents. Also, the snapshots of moisture distribution were presented for intuitive discussion. The dynamic distribution characteristics of moisture were further utilized to explain the effect of moisture contents on CO_2/CH_4 adsorption capacity, adsorption selectivity, specific adsorption energy and isosteric heat. Lastly, the implications of the effect of organic type and moisture content on CS-EGR efficiency were concluded. This work is hoped to gain deep sights into the CO_2/CH_4 competitive adsorption behaviors associated with CS-EGR process, wherein the effect of organic type is expected to help evaluate the CO_2 sequestration site, while the effect of moisture content can provide applicable guidelines for the design of CS-EGR treatment process.

2. Computational methodology

2.1. Kerogen structure units

In this work, we focus on three main immature types of organic matter according to the classification of Tissot and coworkers [22]. Immature kerogens are selected for discussion, since different organic types converge to similar compositions and structural features at high mature stage [54], concealing the effect of organic types on CO_2/CH_4 adsorption. This selection allows us to cover sources of both conventional and unconventional hydrocarbon resources, as summarized below [23].

- Kerogen type IA is derived from the immature Green River shale, typical of hydrogen-rich kerogen deposited in excellent preservation conditions like anoxic lacustrine environments. This kerogen type is especially correlated with oil shale retorting and shale oil.
- Kerogen type IIA is from the Duvernay series, representative of oil-prone shale kerogen deposited in marine environments. This kerogen type is generally regarded as typical source of conventional hydrocarbon resources.
- Kerogen type IIIA is representative kerogen derived from higher plants in organic-rich shale and coal deposited in deltaic environments. Kerogen type IIIA is also important contributing source of conventional oil and gas resources.

Kerogen structure units (Fig. 1) of the three immature organic types adopted in this work were developed by Ungerer et al. [23] based on gathered analytical experimental data from the work of Kelemen and coworkers [54]. Detailed compositions, functional groups and structural parameters of these kerogen units match fairly well with the experimental results of C^{13} NMR spectroscopy, X-ray photoelectron spectroscopy and S-XANES data (Table 1) [54].

2.2. Construction of kerogen molecular models

In this work, a combination of geometry optimization and molecular dynamics simulations is utilized to generate the condensed kerogen models of different organic types using the Materials Studio software [55] with COMPASS force field [56]. This all-atom force field adopts the condensed-phase optimized molecular potential of Lennard-Jones 6–9 to describe the dispersion-repulsion interactions between atomic pairs [56]. It is well known for its high accuracy in predicting thermodynamic properties of condensed phase for both inorganic and organic materials [57].

Geometry optimization and annealing dynamics are initially performed to relax the kerogen model units before the construction of bulk kerogen models [58]. Geometry optimization can find the relaxed structure with local minimal energy, while annealing dynamics aim at finding the stable structure with global minimal energy. Geometry structures of kerogen model units are optimized by the smart minimization algorithm with a fine convergence criterion. Atom-based nonbonded interaction with a fine cutoff distance of 15.5 Å is adopted for the Coulomb and Van der Waals energy summation [58]. The annealing dynamics simulations are carried out using the canonical ensemble (NVT) [57]. We adopt 10 annealing cycles with increasing temperature

Table 1
Compositions and functional groups of the immature kerogens of different organic types.

Property	Parameter	IA		IIA		IIIA	
		Experiment data	Model unit	Experiment data	Model unit	Experiment data	Model unit
Composition	H/C	1.53	1.53	1.17	1.17	0.87	0.89
	O/C	0.051	0.052	0.097	0.095	0.111	0.116
	N/C	0.029	0.028	0.029	0.024	0.017	0.017
	S/C	0.014	0.012	0.014	0.012	0.002	0.000
C group	Aromatic C from XPS(a) or NMR(b) (%)	29(a), 25(b)	29	40(a), 40(b)	41	52(a), 57(b)	57
	C atoms (per aromatic cluster)	16.0	14.6	12.0	11.4	16.0	16.5
	Fraction of attached aromatic C	0.40	0.40	0.43	0.46	0.35	0.36
	Protonated aromatic C (per 100 C)	7.0	6.3	13.0	14.0	21.0	18.0
O group	O in C-O groups (per 100 C)	3.8	4.0	5.0(a), 7.0(b)	5.2	7.0	6.5
	O in carboxylic groups (per 100 C)	0.8	0.8	1.3	1.6	2.1	2.4
	O in carbonyl groups (per 100 C)	0.5	0.4	3.4	2.8	4.0	3.0
N group	Pyrrolic (mol% of N)	57	72	52	66	57	50
	Pyridinic (mol% of N)	20	14	27	17	31	50
	Quaternary (mol% of N)	13	14	18	17	11	0
S group	Aromatic S (mol% of S)	35–45	33	46	67	42	0
	Aliphatic S (mol% of S)	55–65	67	54	33	58	0

from 300 to 800 K and a total simulation time of 400 ps to obtain the stable structures with the lowest energy.

Subsequently, we integrate 6–7 optimized kerogen model units into an amorphous cell to construct initial structure configurations of bulk kerogen models. The amorphous cell is a big simulation box with the target density being 0.1 g/cm^3 [23,59,60]. These initial configurations are thereafter relaxed by a succession of MD simulations, and the relaxation process refers to the procedure reported by previous researchers [23,59,60]. High temperature structural relaxation with NVT ensemble for these initial configurations is firstly carried out at 800 K for 400 ps. Then we perform succeeding MD simulations with NPT ensemble at 20 MPa with a stepwise decreasing temperature from 800 to 300 K [60]. To guarantee the density convergence of kerogen models, simulation time of 400 ps with the time step of 1 fs is adopted for each NPT run. Furthermore, these optimized configurations are simulated at 338 K and 20 MPa for 1 ns to obtain the stable structures. In this work, moist kerogen models are constructed by the fixed loading task in Sorption module of Materials Studio, as adopted in the work of Liu et al. [51]. To be consistent with the kerogen moisture of previous experimental investigations [61] and simulation work [59,62], moist kerogen models of different organic types with a series of moisture contents (0.6, 1.2, 1.8 and 2.4 wt%) were generated in this work.

2.3. Simulation details

The GCMC method with COMPASS force field is used in this work to investigate the competitive adsorption behaviors of CH_4 and CO_2 on dry and moist kerogen models. A detailed description of the GCMC method has been reported in the work of Zhang et al. [44]. The Van der Waals interactions are calculated by the atom-based method with a fine cutoff distance of 15.5 Å, while the Coulombic interactions are summed by the Ewald method [57]. The Andersen thermostat method is adopted to maintain the system temperature. A total of 2×10^7 Monte Carlo steps are performed for each pressure point of the adsorption isotherm, wherein the first 1×10^7 equilibrium steps are utilized to relax the system, while another 1×10^7 production steps are used as statistics to calculate the adsorption amount [57,63]. The method of GCMC simulation outputs the absolute adsorption amount as a function of fugacity rather than pressure. The fugacity of each component in the CO_2/CH_4 gas mixtures is converted from pressure through a combination of the Dalton law and Peng-Robinson equation [64]. To validate the simulated results with experimental data, the simulated absolute adsorption capacity for single component is converted to excess adsorption capacity by,

$$n_e = n_a - \upsilon\rho \tag{1}$$

In this work, the free pore volumes of kerogen models are computed by the method of probe insertion with the Atom Volumes & Surface tool in Materials Studio. A given probe molecule of fixed Connolly radius is utilized to detect the free pore volumes. The probe molecule is randomly inserted into the kerogen system, and rolls over the van der Waals surface of the kerogen skeleton. The surface of the solid skeleton is thus determined, and the regions wrapped by the skeleton surface are identified as free pore volumes [65]. Moreover, we adopt a series of spherical probes of stepwise increasing Connolly radius to detect the corresponding free pore volumes. Accordingly, the pore size distributions of kerogen models are computed by differentiating the free pore volumes with respect to different diameters of probe molecules.

Our work aims at the CO_2/CH_4 competitive adsorption behaviors under different kerogen types and moisture contents. The relative adsorption priority between CH_4 and CO_2 can be reflected by the adsorption selectivity in the binary mixtures, which is defined as [51],

$$S_{CO_2/CH_4} = \frac{x_{CO_2}/x_{CH_4}}{y_{CO_2}/y_{CH_4}} \tag{2}$$

It should be noted that CO_2 is preferably adsorbed on the kerogen models when $S_{CO_2/CH_4} > 1$, and a higher selectivity indicates a stronger adsorption capacity of CO_2 over CH_4.

To study the distinction of thermodynamic property between CH_4 and CO_2 in the mixtures, we calculate the isosteric adsorption heat, which can be determined by the Clausius-Clapeyron equation [66],

$$Q_{st} = RT^2\left(\frac{\partial \ln p}{\partial T}\right)_n \tag{3}$$

To further investigate the interaction strength between CH_4/CO_2 and kerogen, specific adsorption energy is defined as the ratio of the total adsorption energy to the number of adsorbed molecules, which is utilized to reflect the average adsorption energy of a single molecule. The specific adsorption energy is computed in this study by [51],

$$E_a = \frac{(E_{AB} - E_A - E_B)}{N} \tag{4}$$

For molecular simulation techniques, the sources of uncertainty are comprised of both systematic error and random error. The systematic error for MD simulation is related to the simulation time, while that for GCMC simulation is correlated with the sampling step. In this work, sufficient simulation time and sampling step were adopted to eliminate the systematic error by referring to documented simulation details [23,57,59,60,63]. The random error is mainly generated by the initial configuration of kerogen model. In order to reduce the uncertainty brought by random error, four different initial configurations for each kerogen model were constructed, and the simulation results of all configurations were averaged to represent the authentic results. In addition, the standard deviation, indicated by the error bars in the plot, is computed to reflect the uncertainty brought by initial configuration.

3. Results and discussion

3.1. Validation of kerogen models

As shown in Table 1, the compositions and functional groups of the kerogen units used in this work are in good agreement with the experimental results. Furthermore, we validate the condensed-phase kerogen models by comparing the kerogen density, porosity and CH_4 excess adsorption isotherm between simulated results and experimental data.

The density of our immature kerogen IA model at ambient conditions is 0.98 ± 0.01 g/cm^3, which is fairly close to the experimental density for Green River Shale kerogen reported by Facelli et al. [67] (0.95 g/cm^3). The simulated density of kerogen IIA model at ambient conditions (1.11 ± 0.01 g/cm^3) is consistent with the density range (1.0–1.15 g/cm^3) of the immature type II kerogen from the New Albany Shale [68]. The density of kerogen IIIA is 1.14 ± 0.02 g/cm^3, consistent with the known trend by Ungerer et al. [23] that density increases with decreasing H/C ratio for low mature kerogen (IA < IIA < IIIA).

In this work, we utilize helium probe to compute the porosities of kerogen models so as to compare with experimental results. The porosities of kerogen IA and IIA are 12.13 ± 0.1 and 13.25 ± 0.1%, respectively, consistent with the measured porosities (12.5 and 13.8%) for low mature type I-II kerogens of Posidonia Shales by helium pycnometry [69]. The porosity of kerogen IIIA model is 21.00 ± 0.3%. The porosities of our kerogen models are in the range of reported porosities (4.45–22.50%) calculated within organic matter in Barnett mudstone from SEM images [70], which further validates the reliability of our kerogen models.

The CH_4 excess adsorption isotherms of our kerogen models are computed using the method in Section 2.3, and compared with documented experimental results at 338 K (Fig. 2). The measured CH_4 adsorption data in laboratory are performed on type III Cameo coal sample (R_o = 0.56%) [71], type I-II Posidonia shale sample (R_o = 0.50%) [72] and kerogen samples (R_o = 0.53%) [69]. These

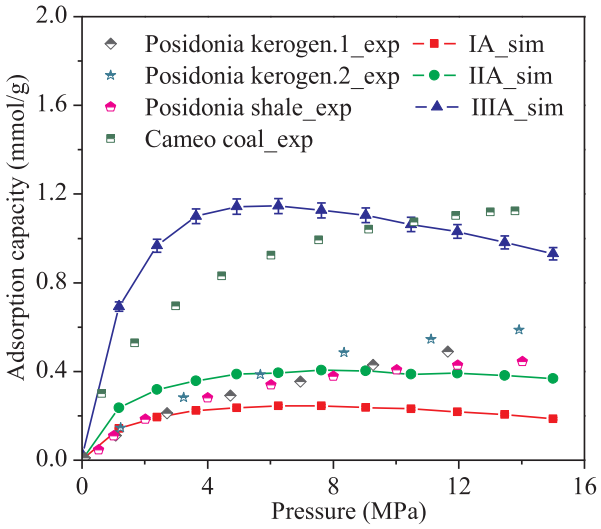

Fig. 2. Comparison of CH_4 excess adsorption isotherms between simulated results and experimental data at 338 K.

experimental data are normalized by TOC to relieve the effect of inorganic matter. It should be noted that comparison of gas adsorption isotherms from different samples-even for samples within the same region-is difficult due to the discrepancies in sample preparation and sample properties including maturity, organic type and inorganic content. By performing the comparison in Fig. 2, what we expect is to check the reasonability rather than the accuracy for our kerogen models to match with documented experimental data. As seen in Fig. 2, although our simulated CH_4 excess adsorption isotherms cannot be perfectly fitted by the documented experimental data, the magnitude of CH_4 excess adsorption capacity is fairly close to the experimental results. The maximum CH_4 excess adsorption capacity for type III kerogen (1.14 ± 0.034 mmol/g) is fairly consistent with the normalized experimental result of Cameo coal (1.12 mmol/g) at 13.8 MPa. Also, the simulated CH_4 excess adsorption isotherms for type I and type II kerogen models are in good agreement with the normalized experimental results on Posidonia shale and kerogen samples. Moreover, the simulated CH_4 excess adsorption capacity is in the order of kerogen type I < type II < type III, which is consistent with the reported experimental conclusion by Zhang et al. [71]. Differences between experimental and simulated CH_4 excess isotherms in Fig. 2 can be explained by the issue of pore accessibility. As reported in previous investigations [73–77], realistic heterogeneous porous material such as shale and kerogen sample possesses the pore accessibility problem for adsorbates due to the presence of impenetrable pore necks between theoretically enterable pores. Under low temperature and pressure conditions, gas adsorbates do not have sufficient energy to overcome the activation energy barriers, so they cannot pass through the pore necks [74]. Thus, a large amount of inaccessible pores remain to be potentially occupied by gas molecules. With increasing temperature or pressure, on one hand, the chemical potential of gas molecules increases, providing additional energy for gas molecules, on the other hand, the pore necks can be enlarged, reducing the activation energy barriers [75]. The combined two factors lead gas molecules to enter the originally inaccessible pores, which causes an anomalous increase of gas adsorption amount. Actually, this could be one reason why the experimental CH_4 excess isotherms in Fig. 2 do not show the maximum. However, it should be noted that for the GCMC method, the random insertion of gas molecules based on massive probability statistics is utilized to simulate the adsorption amount. It means that the effect of impenetrable pore neck is neglected during the simulation process. That is why the simulation results in Fig. 2 show higher CH_4 excess adsorption capacities than corresponding experimental results at low pressure conditions. Moreover, since the structure of adsorbent remains fixed during the gas adsorption process, the subtle swelling in microstructure due to increasing pressure is also neglected for the GCMC simulation. Accordingly, the maximum CH_4 excess adsorption capacities are observed in the simulated isotherms in Fig. 2, since there is no additional pore volume for gas adsorption. Furthermore, differences between simulated and experimental results can be also attributed to the discrepancy in sample property, especially the molecular structure and inorganic content. This is because our kerogen models are not directly derived from the experimental samples used for comparison in Fig. 2 due to limited experimental data in the literature. For CH_4 excess adsorption capacity, the uncertainty on type I and type II kerogen can be neglected, since the error bars are smaller than the symbols. By contrast, there are observable deviations for type III kerogen, and the standard deviation can be up to 0.034 mmol/g. However, this uncertainty is acceptable, because the uncertainty for different configurations is within ± 3%.

3.2. Effect of organic type on mixed gases adsorption

3.2.1. Effect of pore structure characteristics

Initially, absolute adsorption isotherms of CH_4 and CO_2 in the binary mixtures on dry kerogen models of different organic types at 338 K are simulated using the GCMC method (Fig. 3). The absolute adsorption isotherms are averaged by four different configurations for

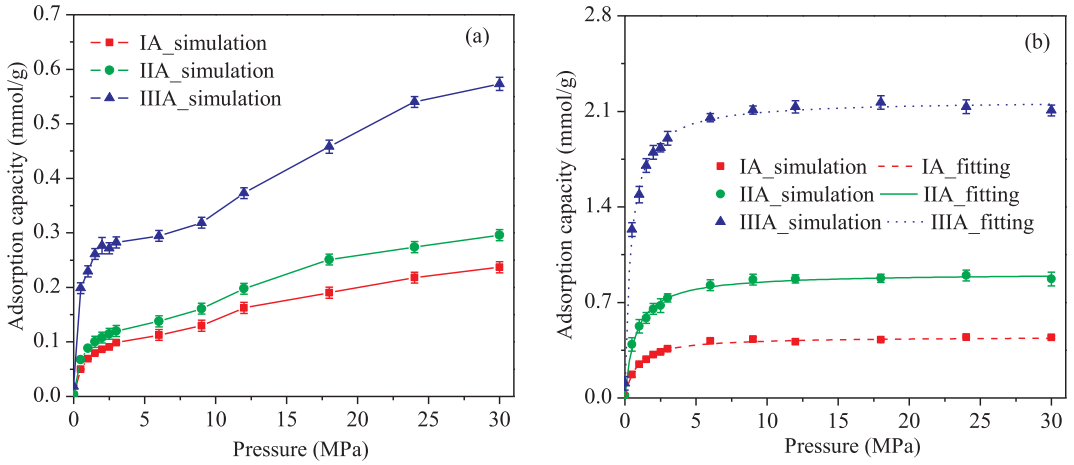

Fig. 3. Absolute adsorption isotherms of CH_4 and CO_2 in the binary mixtures on dry kerogen models of different organic types at 338 K with y_{CO_2} = 0.5. (a) CH_4 absolute adsorption isotherms; (b) CO_2 absolute adsorption isotherms.

each kerogen model to reduce the simulation uncertainty. The CH_4 absolute adsorption isotherms are found to follow a trend of step-wise isotherm, which belongs to the type VI isotherm according to the classification of Gregg and Sing [78]. Particularly, two steps are observed for these CH_4 isotherms, and the second step is less steep than the first one. By contrast, The CO_2 absolute adsorption isotherms correspond to the type I isotherm, and can be fairly fitted by the Langmuir model. The CO_2 adsorption capacity is much bigger than that of CH_4, indicating that CO_2 is preferably adsorbed in the kerogen models. The kerogen model is physically heterogeneous, with its surfaces composed of inner surfaces and outer surfaces of micropores. As shown in Fig. 4a, CH_4 molecules are preferentially adsorbed on the inner surfaces of the kerogen model for single component adsorption. As for CO_2/CH_4 competitive adsorption, CO_2 molecules are observed to occupy the inner surfaces of micropores, while CH_4 molecules are adsorbed on both the inner surfaces and the outer surfaces due to weaker adsorption capacity (Fig. 4b). Thus, we can infer that the first step on the step-wise CH_4 isotherm corresponds to CH_4 adsorption on the inner surfaces, and the second one corresponds to that on the outer surfaces. The first step is steeper owing to the larger surface areas and stronger adsorption potentials of inner surfaces. By contrast, the distinction between the interior and exterior sites is not significant in the CO_2 isotherm (Fig. 3b), since most of CO_2 molecules are preferentially adsorbed on the high-energy interior sites for CO_2/CH_4 competitive adsorption, as shown in Fig. 4b. In the system of kerogen and mixed gases, CO_2 can displace CH_4 from the inner surfaces to the outer surfaces, thus facilitating the production of CH_4 from unconventional gas reservoirs. The standard deviations show a relatively good reproductivity (within 0.045 mmol/g) for the CH_4 and CO_2 absolute adsorption capacity in the mixtures. The uncertainty on CO_2 adsorption is more significant than that on CH_4 adsorption. Besides, the uncertainty is observed to increases with the pressure.

Furthermore, the order of adsorption capacity for both CH_4 and CO_2 on different kerogen models is type I < type II < type III (Fig. 3). Gas adsorption capacity is associated with both the functional groups [79] and the microporosity of kerogen [71]. The O/C ratio of our kerogen models is 5.2, 9.5 and 11.6% for kerogen IA, IIA, and IIIA, respectively, which is consistent with the reported conclusion that gas adsorption capacity increases with the O/C ratio [79]. Also, the porosities probed by helium molecule for our kerogen IA (12.13 ± 0.1%), IIA (13.25 ± 0.1%) and IIIA (21.00 ± 0.3%) are proportional to the gas adsorption capacity in the mixtures.

To further investigate the effect of pore structure characteristics on gas adsorption capacity, we compute the pore size distributions and the contributions of different kinds of pores to the total pore volumes (Fig. 5). Pore size distributions of our kerogen models show a mono-peak type, with the pore width corresponding to the peak site at ~1.6 Å. The pore size distributions of kerogen IA and IIA models are relatively more concentrated, while that of kerogen IIIA model is more uniform. In this work, the pores less than 4 Å are defined as ineffective pores, which are not accessible for gas molecules, while those pores bigger than 4 Å are defined as enterable pores. As indicated in Fig. 5, the pore networks of our kerogen models are comprised of massive ineffective pores and a small number of enterable pores. These ineffective pores and narrow pore necks are correlated with the gas transport limitation, while these enterable pores are relevant to the gas adsorption capacity. The averaged fraction of enterable pores to the total pore volumes is 9.38, 13.59 and 28.88% for kerogen IA, IIA and IIIA models, respectively, which is consistent with the gas adsorption capacity (Fig. 3). The pore structure characteristics under different initial configurations diverge slightly, with the uncertainty of pore volumes less than 6.67%.

3.2.2. Effect of surface chemically heterogeneity

In this section, we aims to investigate the effect of surface chemically heterogeneity on mixed gas adsorption on kerogen models. The CO_2/CH_4 adsorption selectivity on our kerogen models of different organic types as a function of pressure is presented in Fig. 6. The simulated results of selectivity (1.87–6.97) are fairly close to the reported values on coal (2.3–8.9) [44]. These values of selectivity are always larger than 1, which indicates that CO_2 has a larger adsorption capacity than CH_4 to be preferentially adsorbed on the kerogen models, as discussed in Section 2.3. Consistent trend for the three kerogen models can be observed that the selectivity initially increases with pressure, then decreases quickly and finally tends to reach a constant. This trend has also been reported by Zhang et al. [44] and Dang et al. [80] for CO_2/CH_4 competitive adsorption on coal. Kerogen is energetically heterogeneous. The adsorption sites with stronger energy are preferentially occupied by CO_2 molecules at low pressure. As the pressure increases, CO_2 and CH_4 begin to competitively occupy the lower energy sites once

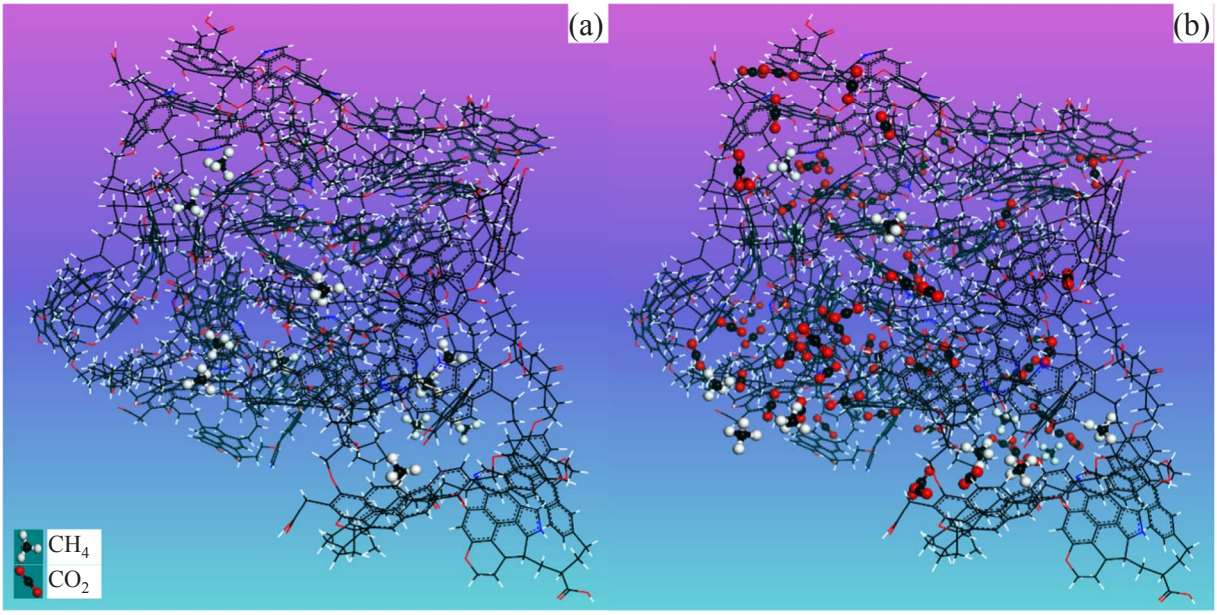

Fig. 4. Snapshots of gas molecules distribution in kerogen IIIA model at 338 K. (a) Single CH_4 loading with fixed 11 molecules; (b) mixed CH_4 and CO_2 loading at 30 MPa with $y_{CO_2} = 0.5$. Atom representations refer to Fig. 1.

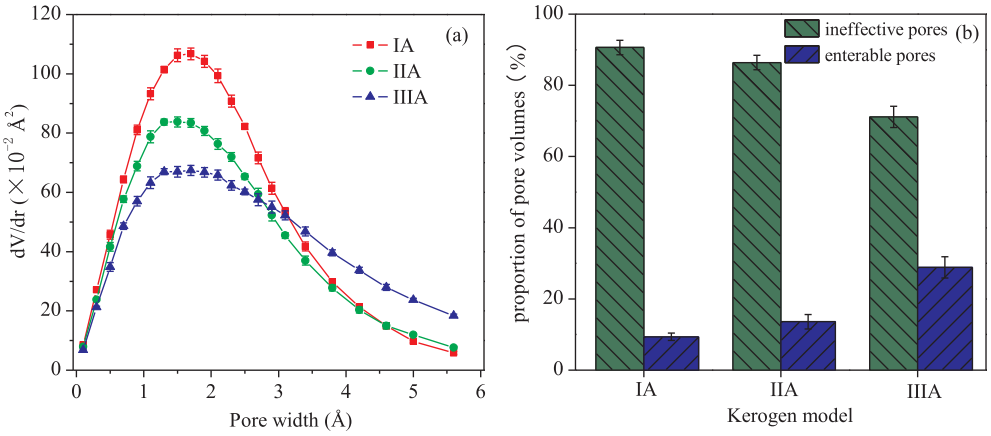

Fig. 5. (a) Pore size distributions; (b) contributions of different kinds of pores to total pore volumes.

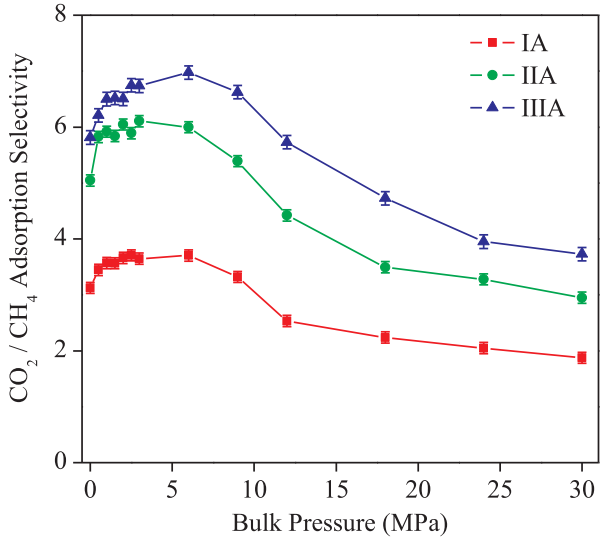

Fig. 6. CO_2/CH_4 adsorption selectivity on kerogen models as a function of pressure.

the higher energy sites are filled. That is why the selectivity is higher at low pressure and lower at high pressure. Moreover, we observe the maximal adsorption selectivity at ~6 MPa, which is consistent with the finding in the work of Zhang et al. [44]. The sequence of selectivity for kerogen models of different organic types is type III > type II > type I. This observation can be explained by the pore structure characteristics of the kerogen models. As shown in Fig. 5, the proportion of ineffective pores is in the order of type I > type II > type III. The increasing ineffective pores lead to a rapid decline of accessible high energy sites due to the transport limitation of inaccessible pores, resulting in a lower adsorption selectivity. The divergence of selectivity among different initial configurations is relatively small, which indicates a good reproductivity. The uncertainty is in the order of type III > type II > type I.

The isosteric heat of CH_4 and CO_2 adsorption is computed to study the interaction between CH_4/CO_2 and kerogen, and the results are presented in Fig. 7. The isosteric heat of CO_2 is larger than that of CH_4, indicating that the kerogen models have a higher affinity for CO_2 compared with CH_4. The isosteric heat of CO_2 increases at the beginning, and then changes gently as the pressure increases. The initial increase of CO_2 isosteric heat corresponds to the significant increase of interaction energy of kerogen-CO_2 at low pressure, as reported by Zhang et al. [44]. It should be noted that the isosteric heat of gas adsorption is contributed by both the adsorbate-adsorbent interaction and the adsorbate-adsorbate interaction [57]. On one hand, gas molecules tend to occupy the energetically weaker sites with increasing pressure, decreasing the isosteric heat. On the other hand, the adsorbate-adsorbate interaction increases with the adsorption amount, increasing the isosteric heat. Therefore, the gentle change of isosteric heat at high pressure is the combined results of the above two factors. Moreover, we observe a decrease stage for the isosteric heat of CH_4 in the pressure range between 1.5 and 6 MPa. This may because that part of CH_4 molecules are expelled from the inner surfaces to the energetically weaker outer surfaces of micropores, as shown in Fig. 4b. Similar with the absolute adsorption capacity, the isosteric adsorption heat for CH_4 and CO_2 in the mixtures also presents a good reproductivity under different configurations. Type III kerogen has the largest standard deviations, but the deviations are still in the range of 0.15–0.30 kJ/mol. The uncertainty is acceptable.

The radial distribution function (RDF) is defined as the loading probability of a certain particle as a function of distance from a reference particle, which can reflect the affinity between the two particles. We compute the RDFs between CH_4/CO_2 and atoms in our kerogen models (C, H, O, N, S) to find the possible high energy adsorption sites (Fig. 8). The close contact peak between CH_4 and S in kerogen IA and IIA models is shaper than these between CH_4 and other atoms, while the first peak between CH_4 and N in kerogen IIIA model is the highest peak. This observation suggests that sulfur-containing functional groups are the high energy sites for CH_4 in kerogen IA and IIA models, while nitrogen-containing functional groups are the high energy sites for CH_4 in kerogen IIIA model. For our immature kerogen models, oxygen-containing functional groups have a weaker affinity for CH_4, which is consistent with previous conclusion made by Zhang et al. [44]. By

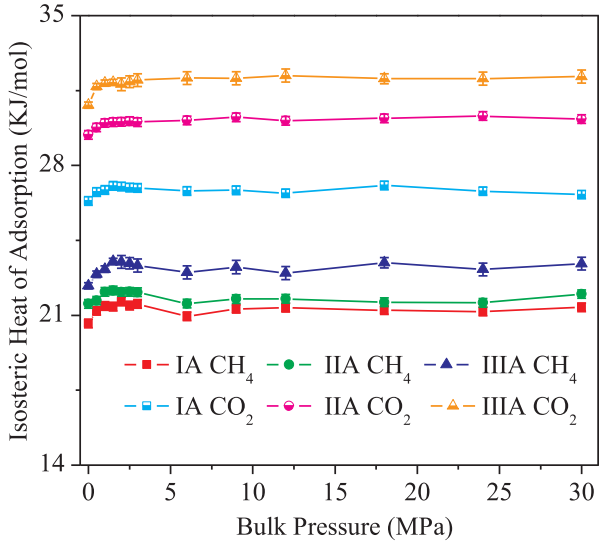

Fig. 7. Isosteric heat of CH_4 and CO_2 adsorption in kerogen models at 338 K.

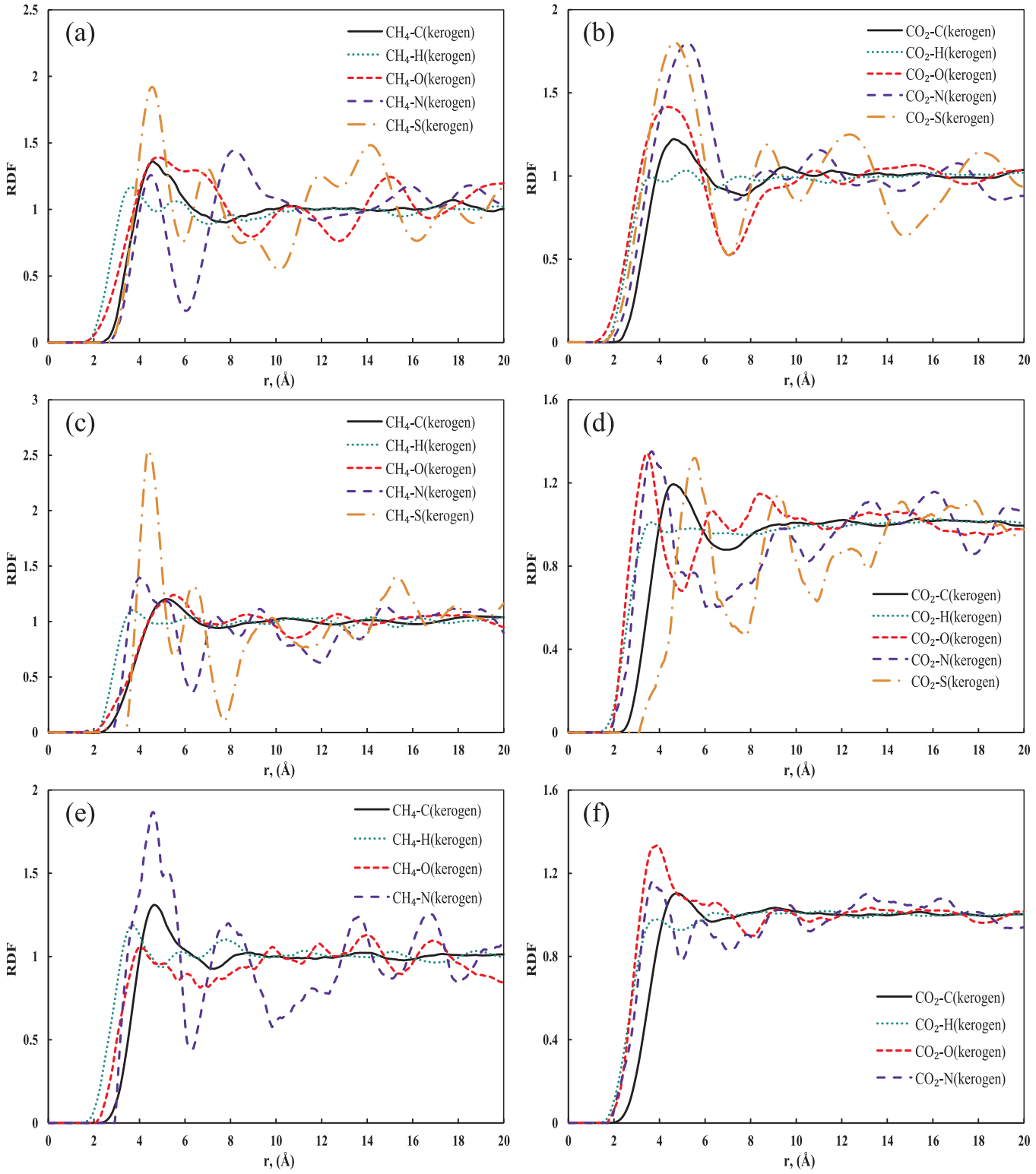

Fig. 8. Average radial distribution functions (RDFs) between CH_4/CO_2 and atoms in our kerogen models (C, H, O, N, S). (a) CH_4 in kerogen IA model; (b) CO_2 in kerogen IA model; (c) CH_4 in kerogen IIA model; (d) CO_2 in kerogen IIA model; (e) CH_4 in kerogen IIIA model; (f) CO_2 in kerogen IIIA model.

contrast, the close peaks between CO_2 and sulfur-, nitrogen- and oxygen-containing groups for kerogen IA and IIA models and between CO_2 and nitrogen- and oxygen-containing groups for kerogen IIIA model are significant, which indicates that our kerogen models have more high energy sites for CO_2 adsorption. Moreover, the relative affinity between CO_2 and oxygen-containing groups increases from kerogen IA model to kerogen IIIA model. The oxygen-containing groups are preferentially occupied by CO_2, which has also been reported by Dang et al. [80]. We can infer that the sulfur-containing groups in kerogen IA and IIA models and the nitrogen-containing groups in kerogen IIIA model are the main competitive adsorption sites for CH_4 and CO_2.

3.3. Effect of moisture on mixed gases adsorption

3.3.1. Distribution of H_2O molecules

To understand the effect of moisture on CO_2/CH_4 competitive adsorption, it is essential to study the distribution of H_2O molecules in the kerogen models. In this work, we firstly derive the distribution of H_2O molecule by analyzing the change of pore size distributions of kerogen models under different moisture contents (Fig. 9). It can be observed that the volumes of enterable pores decrease, while the volumes of ineffective pores increase with increasing moisture content. This observation indicates that H_2O molecules enter the accessible pores and divide them into many ineffective pores. It can be also noted that the distribution of H_2O molecules covers most of the accessible pores, as volumes of these pores decrease with increasing moisture content. Moreover, moisture is observed to have a bigger effect on these pores with bigger diameters. This is because that the transport limitation of these pores for H_2O molecules is less significant, which facilitates the aggregation of H_2O molecules in these pores. As shown in Fig. 9a, nearly all volumes of pores above 5 Å are filled by H_2O molecules for kerogen IA model at 2.4 wt% moisture condition.

To investigate the distribution of H_2O molecules on different functional groups, we compute the RDFs between H_2O and atoms in the kerogen models (Fig. 10). The close peaks between H_2O and S atom and between H_2O and O atom are higher than other peaks for kerogen IA model, while the first peak between H_2O and O atom is the highest peak for kerogen IIA and IIIA models. This suggests that H_2O molecules are mainly distributed around sulfur- and oxygen-containing groups for kerogen IA model and oxygen-containing groups for kerogen IIA and IIIA models. The snapshots of H_2O molecules distribution in kerogen IIA model at different moisture contents are illustrated in Fig. 11. It can be noted that H_2O molecules are preferentially adsorbed on the oxygen-containing groups at low moisture conditions (Fig. 11a). While at higher moisture conditions ((Fig. 11b–d), two distribution forms for H_2O molecules can be observed, namely, most of H_2O molecules aggregate into clusters and distribute in the middle of pores, while a small number of H_2O molecules are adsorbed on the oxygen-containing groups. Fig. 12 presents the pore volume distributions of kerogen IIA model under different moisture contents. Moisture has a small influence on the pore volumes at low moisture content (Fig. 12a and b), because these H_2O molecules are mainly distributed around the oxygen-containing groups of pore walls. By contrast, the pore volumes are greatly affected by moisture at higher moisture content (Fig. 12b and c). This can be attributed to the aggregation of H_2O molecule clusters in the middle of these pores. Particularly, we observe an increase of pore volumes with increasing moisture content at local regions in the kerogen model (Fig. 12c and d), resulting in the re-exposure of oxygen-containing groups initially occupied by H_2O molecules. This finding indicates that some dispersed H_2O molecule can migrate to the clusters at high moisture contents.

3.3.2. Effect of moisture content

In this section, we investigate the influence of moisture content on CO_2/CH_4 adsorption capacity, adsorption selectivity, specific adsorption energy and isosteric heat. Fig. 13 shows the effect of moisture

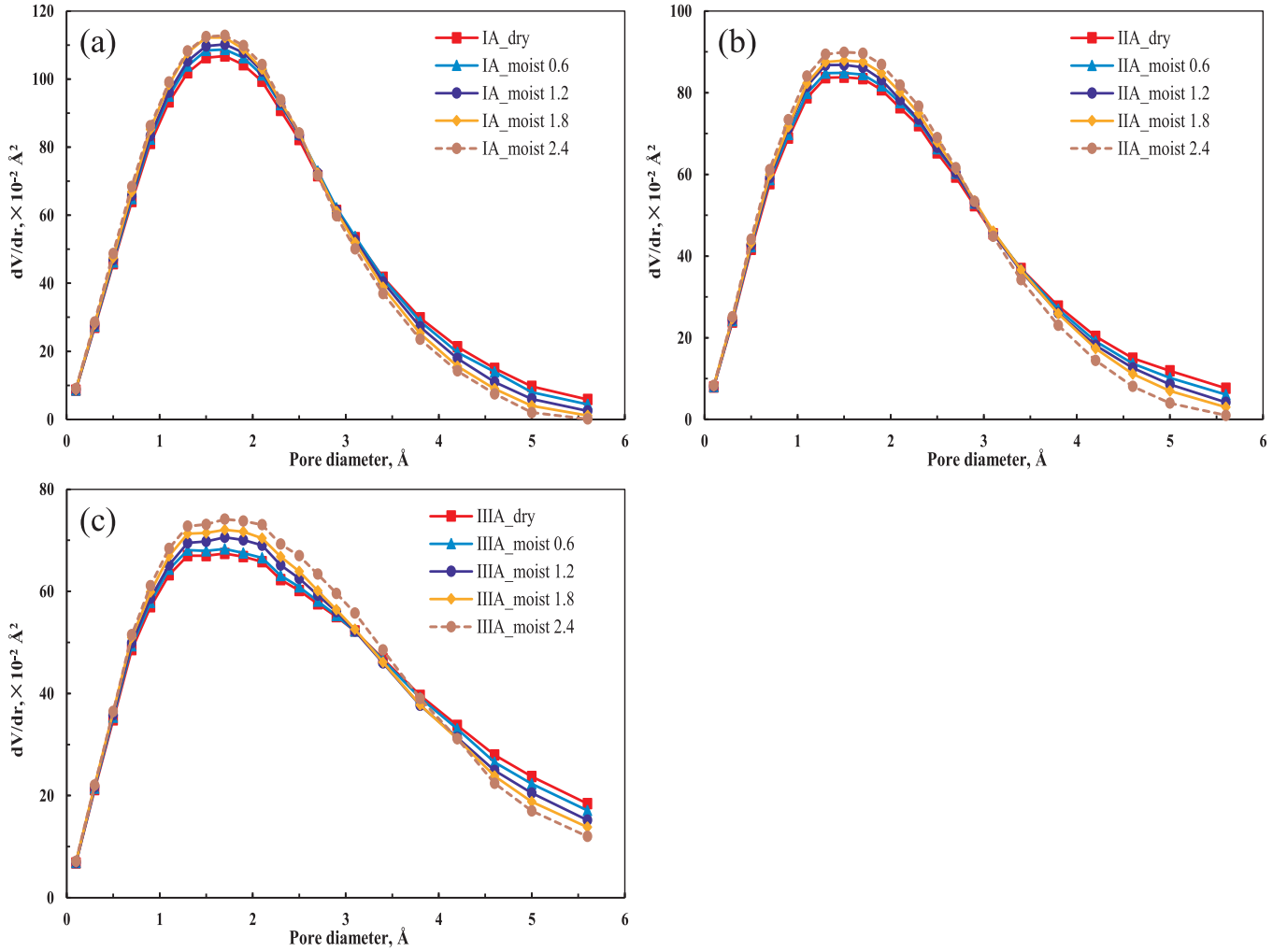

Fig. 9. Effect of moisture content on the pore size distributions of our kerogen models. (a) Kerogen IA model; (b) kerogen IIA model; (c) kerogen IIIA model.

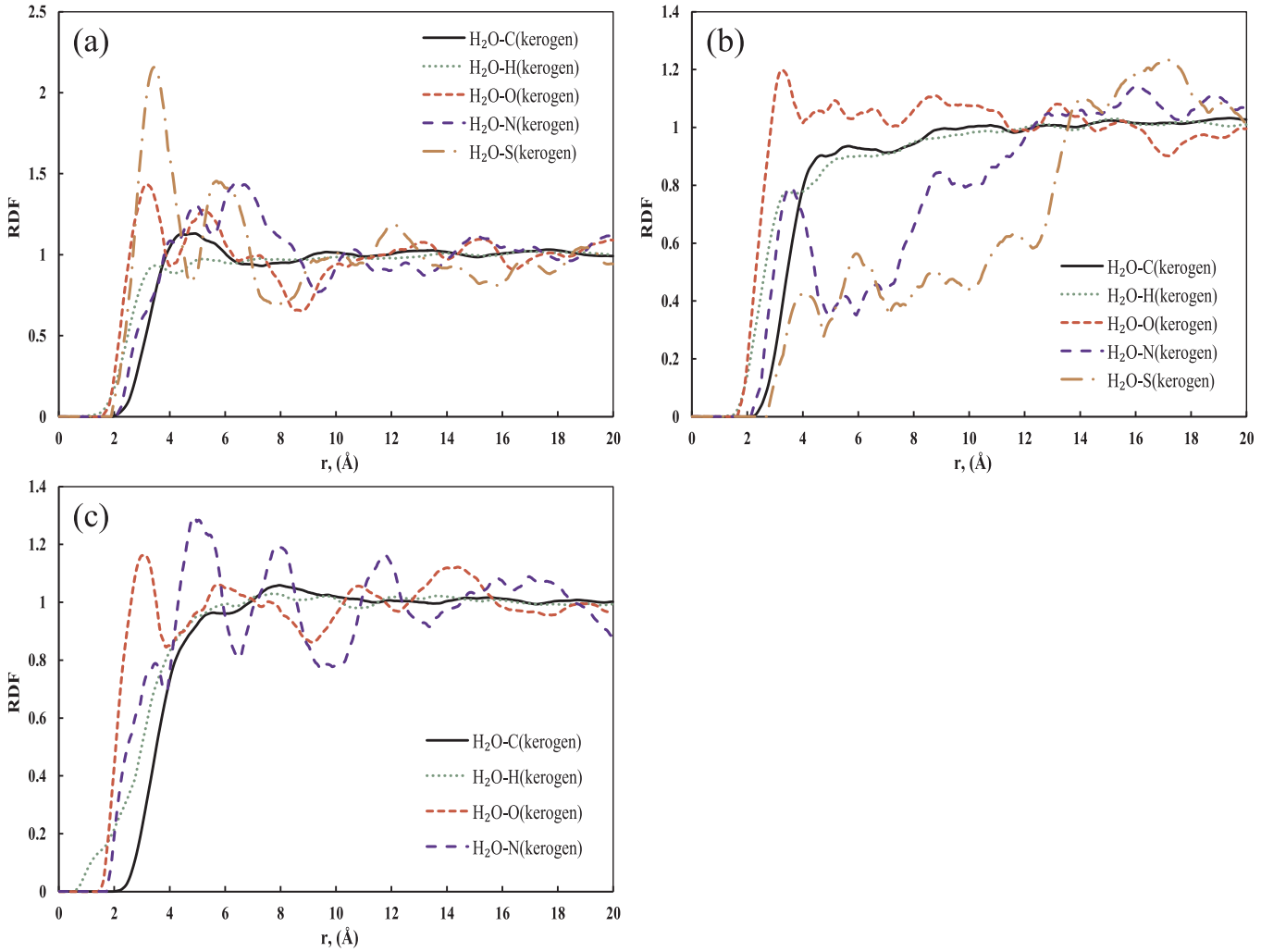

Fig. 10. RDFs between H_2O and atoms in the kerogen models at the moisture content of 2.4 wt%. (a) Kerogen IA model; (b) kerogen IIA model; (c) kerogen IIIA model.

content on CO_2/CH_4 adsorption capacity in the binary mixtures at 30 MPa. It can be noted that CO_2/CH_4 adsorption capacity decreases with the increase of moisture content. For kerogen IA model at the moisture content of 2.4 wt%, the CO_2/CH_4 adsorption capacity drops to a fairly low level, which can be attributed to the occupation of H_2O molecules clusters in the enterable pores. We further compute the CO_2/CH_4 adsorption selectivity under different moisture contents, and the results are presented in Fig. 14. The selectivity decreases in the beginning, and then increases with increasing moisture content. The later increase of selectivity with moisture content has also been reported by Weniger et al. [81]. This trend indicates that moisture has a bigger effect on the adsorption capacity of CO_2 compared with that of CH_4. As discussed in Section 3.3.1, at low moisture conditions, H_2O molecules are preferentially adsorbed around the oxygen- and sulfur-containing groups, which also have higher affinity for CO_2 rather than CH_4, thus decreasing the adsorption capacity of CO_2 with a greater extent. At high moisture conditions, many H_2O molecules migrate and aggregate into clusters in the enterable pores, which exposes many polar groups to be potentially adsorbed by CO_2, leading to a relatively slow decrease of CO_2 adsorption capacity. Fig. 13 suggests that the uncertainty of gas adsorption capacity has no obvious correlation with moisture content. Also, the largest standard deviation (0.064 mmol/g) is observed for type III kerogen, which is still within the acceptable uncertainty (± 3%). Fig. 14 indicates that the uncertainty of selectivity is bigger at high pressure (30 MPa, within ± 5%) than that at low pressure (6 MPa, within ± 3%).

Fig. 15 shows the effect of moisture on the specific adsorption energy between $CH_4/CO_2/H_2O$ and kerogen systems at 30 MPa. The specific adsorption energy is computed to reflect the average adsorption energy of a single molecule with kerogen system. The specific adsorption energy between H_2O and kerogen systems decreases with increasing moisture content, which is due to the gradual aggregation of H_2O molecule into clusters in the enterable pores. The order of specific adsorption energy between H_2O and different kerogen systems is kerogen IA < IIA < IIIA, consistent with the order of O/C ratio and the enterable pore volume fraction (Fig. 5b). For kerogen IIIA model, more enterable pore volumes (Fig. 5b) and better pore connectivity (Fig. 11) are observed, facilitating H_2O molecules to get access to more polar functional groups. The specific adsorption energy between CO_2/CH_4 and kerogen systems initially decreases and then increases with the increase of moisture content. The early decrease can be attributed to the occupation of polar functional groups by H_2O molecules, while the later increase is related to the aggregation and migration of H_2O molecules. Compared with CH_4, the specific adsorption energy between CO_2 and kerogen systems begins to increase at a lower moisture content, which further indicates that moisture has a bigger effect on CO_2 adsorption. This is because that both H_2O and CO_2 have high affinity with oxygen- and sulfur-containing groups. The divergence of specific adsorption energy is also small, indicating a good reproductivity. The largest standard deviation (0.469 kJ/mol) is observed for H_2O-IIIA kerogen at the moisture content of 0.6 wt%.

The effect of moisture on the isosteric heat of CH_4 and CO_2 at

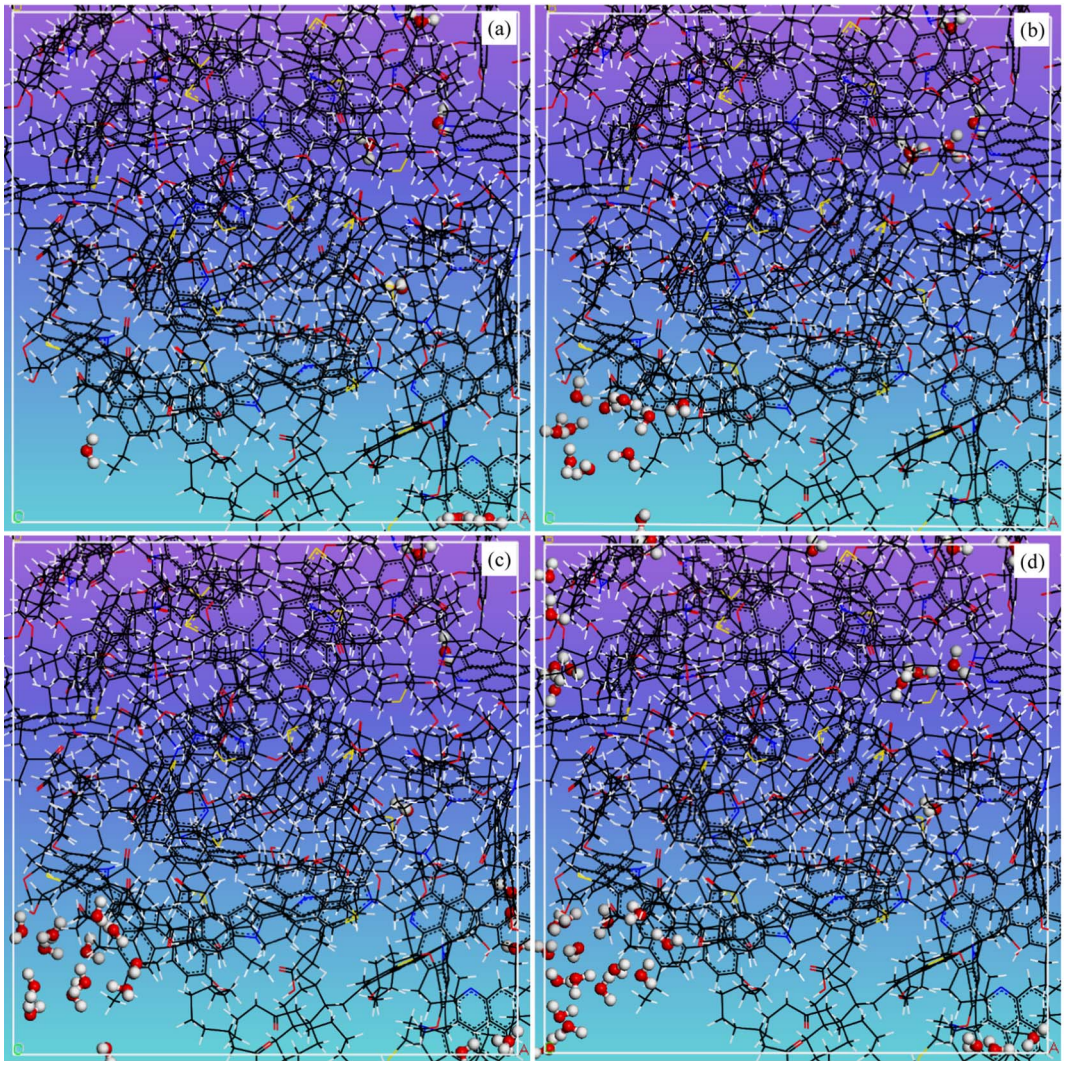

Fig. 11. Snapshots of H_2O molecules distribution in kerogen IIA model at different moisture contents. (a) 0.6 wt%; (b) 1.2 wt%; (c) 1.8 wt%; (d) 2.4 wt%. Atom representations refer to Fig. 1.

30 MPa is illustrated in Fig. 16. Similar with the specific adsorption energy, the isosteric heat of CO_2 also decreases at the beginning, and then increases slowly with the moisture content. While the isosteric heat of CH_4 tends to decreases slowly with the increase of moisture content. With the early increase of moisture content, the isosteric hear of CO_2 drops quickly, while that of CH_4 decreases slowly. This is because H_2O molecules are mainly adsorbed on the oxygen- and sulfur-containing groups at low moisture conditions, and these groups have higher affinity with CO_2 rather than CH_4. The later increase of isosteric heat of CO_2 can be also explained by the re-exposure of polar groups due to the aggregation and migration of H_2O molecules at high moisture conditions (Fig. 12c and d). The uncertainty of gas isosteric adsorption heat does not change with the moisture content. The standard deviation for CO_2 (within 0.32 kJ/mol) is bigger than that for CH_4 (within 0.23 kJ/mol).

3.4. Implication for CS-EGR

This work investigates the effect of organic type and moisture content on the competitive adsorption of injected CO_2 with subsurface CH_4, which is closely related to the CS-EGR efficiency. In this section, we discuss how these results could be utilized to improve the efficiency of CS-EGR technique in field applications.

Our study on the influence of organic type on CO_2/CH_4 competitive adsorption can provide a direct criterion for the site selection for the CS-EGR project with application to shale and coal systems. Bachu et al. [82] have proposed a roadmap for the site selection for CO_2 sequestration in geological media. They concluded that the suitability for long time storage is one of the most important criteria. Based on our investigations, type IIIA kerogen among the three types has the highest storage capacity and adsorption selectivity for CO_2, which facilitates the stable sequestration of CO_2 and the effective displacement of CH_4 at the same time. Thus, type IIIA is the optimized organic type for CS-EGR project. It should be noted that type IIIA kerogen is mainly derived from higher plants in organic-rich shale and coal deposited in deltaic environments. Therefore, the potential of CS-EGR for continental CBM and shale gas reservoirs should be preferentially emphasized.

The effect of moisture content on CO_2/CH_4 adsorption can provide applicable guidelines to help improve the CS-EGR efficiency. Based on our study, by increasing the kerogen moisture content in the reservoir, the CO_2 sequestration capacity is reduced, but the displacement efficiency of CH_4 by injected CO_2 can be potentially enhanced. The implication of this finding for CS-EGR project is that for the same amount of CH_4 produced, less amount of CO_2 is needed to be pumped into the reservoir at the optimum moisture condition. This point is extremely important for CS-EGR project, since the expense of capturing-pressuring-transporting CO_2 is huge in order to inject CO_2 into the underground gas-bearing layers. The original kerogen moisture content,

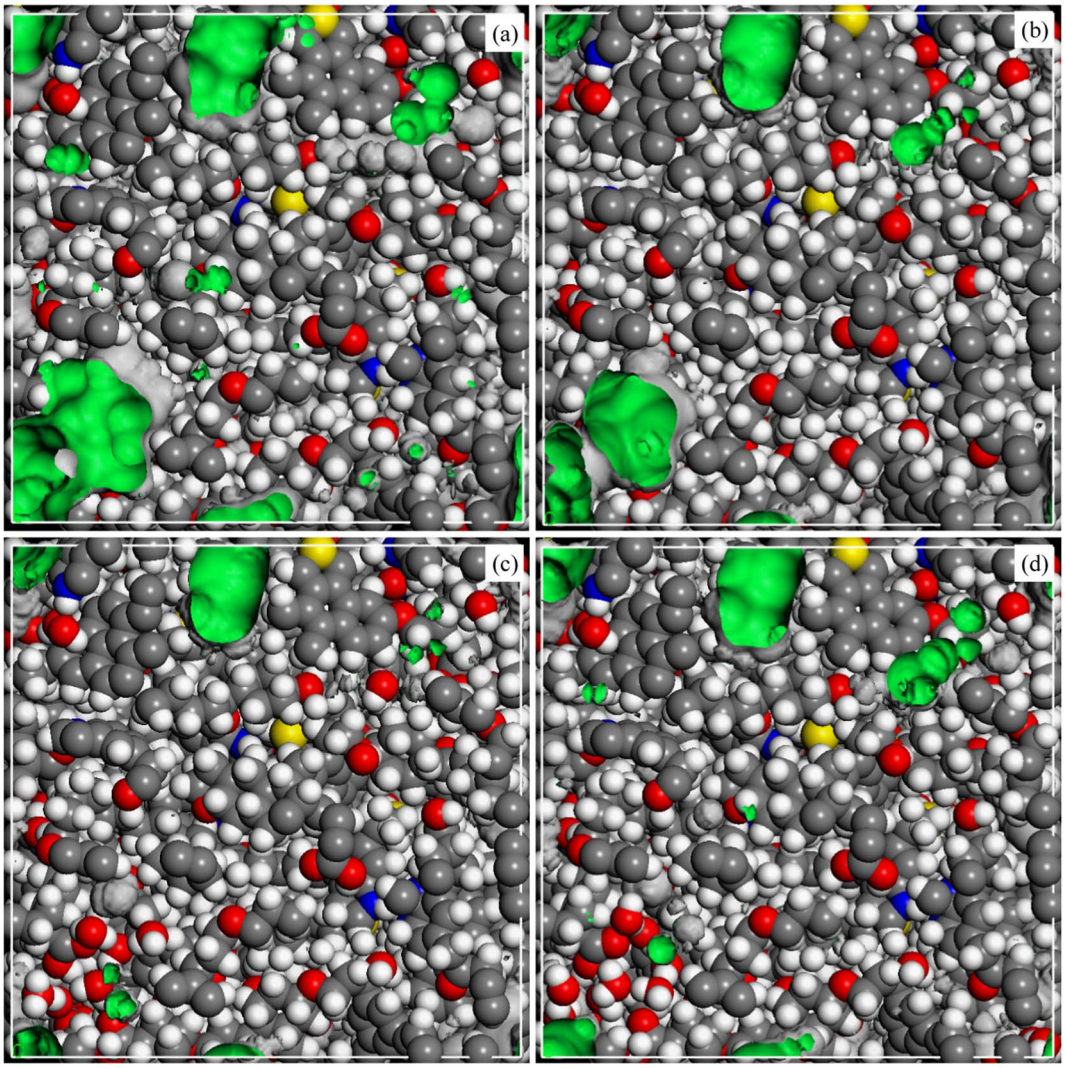

Fig. 12. Pore volumes distributions of kerogen IIA model under different moisture contents. Pore volumes are colored in green. (a) 0 wt%; (b) 0.6 wt%; (c) 1.2 wt%; (d) 1.8 wt%.

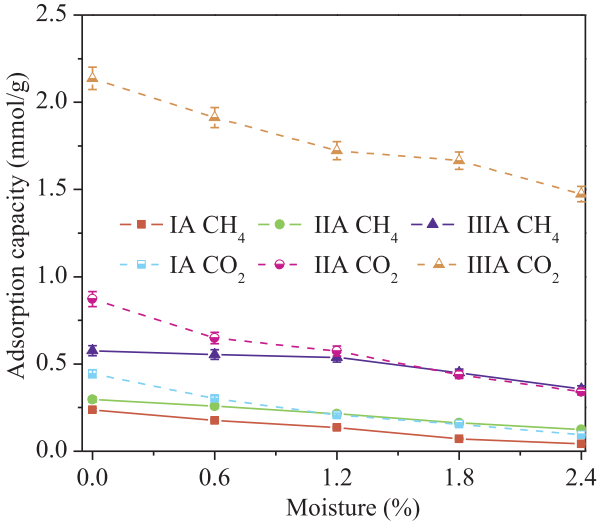

Fig. 13. CH_4 and CO_2 adsorption capacity in the mixtures under different moisture contents at 30 MPa with $y_{CO_2} = 0.5$.

closely correlated with the carboxylic and hydroxylic groups in coal and shale, is relatively low under reservoir conditions, especially for type III kerogen or high mature kerogen on which most of hydrophilic functional groups have been removed. Therefore, it is theoretically feasible to enhance the efficiency of CS-EGR technique with application to these kinds of unconventional gas reservoirs by increasing the kerogen moisture content. At present, CO_2-based fracturing technique is one of the main approaches for injecting CO_2 into underground gas-bearing layers. However, the poor proppant-carrying capacity of CO_2 remains to be improved. Thus, it is instructive that we may utilize the CO_2-based fracturing technique to produce artificial fractures, and then inject water-based fluid to carry proppants to the fractures, which can not only improve the fracturing efficiency, but also potentially increase the moisture content in organic matter. Furthermore, steam injection and reservoir heating are also potential techniques to increase the kerogen moisture content, thus improving the efficiency of CS-EGR.

Moreover, the effect of pressure on the CS-EGR efficiency can provide guidance on the design of injection timing of CO_2. Results of our study indicate that CO_2/CH_4 adsorption selectivity at low reservoir pressures is larger than that at high reservoir pressures for both dry and moist kerogen models of different organic types, and there is optimum pressure (~ 6 MPa) for maximum adsorption selectivity. For unconventional gas reservoirs with deep geological depths, the reservoir pressure decreases with the desorption and production of adsorbed gases. There are still a large amount of residual adsorbed gases in the tight reservoir at low reservoir pressures, which can be further displaced by injected CO_2. Accordingly, based on our investigations, it is suggested that the injection of CO_2 into the reservoir should be

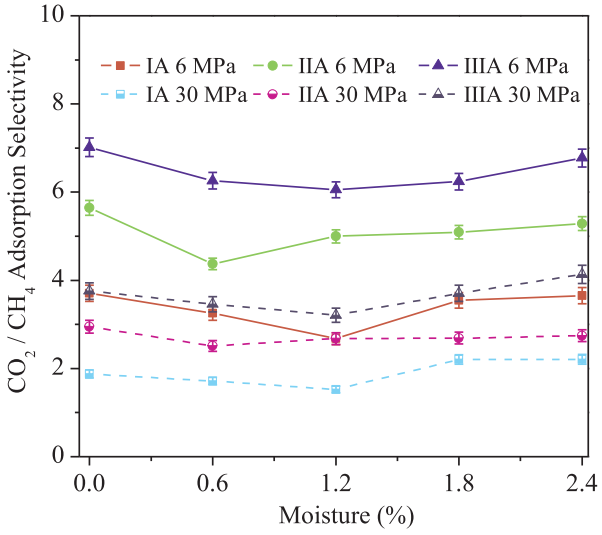

Fig. 14. CO_2/CH_4 adsorption selectivity under different moisture contents with $y_{CO_2} = 0.5$.

implemented after the reservoir pressure drops to a certain degree so as to improve the efficiency of CS-EGR.

4. Conclusions

In this work, three realistic immature kerogen models of different organic types with various moisture contents were generated by combined MD and GCMC simulations. The competitive adsorption behaviors of CH_4 and CO_2 on the dry and moist kerogen models were further investigated. The effect of organic type and moisture content on kerogen pore structure, chemically heterogeneous surface and mixed gas adsorption were discussed in detail, and its implications for CS-EGR were summarized.

Our results indicate that kerogen IIIA is the optimized organic type for CS-EGS. CH_4 absolute isotherms follow a trend of step-wise isotherm, while CO_2 absolute isotherms correspond to the type I isotherm for the binary mixtures. The CO_2/CH_4 adsorption capacity and adsorption selectivity are in the order of kerogen IA < IIA < IIIA, which is consistent with the sequence of averaged enterable pore volume fraction (IA, 9.38%; IIA, 13.59%; IIIA, 28.88%). The enterable pore volume is positively correlated with the gas storage capacity, while the ineffective pore volume is relevant to the transport limitation for small molecules. The sequence of relative affinity between CO_2 and oxygen-containing groups is kerogen IA < IIA < IIIA.

Two distribution forms for H_2O molecules can be concluded. At low moisture conditions, H_2O molecules tend to occupy sulfur- and oxygen-containing groups in kerogen IA, and oxygen-containing groups in kerogen IIA and IIIA, while at high moisture conditions, H_2O molecules tend to migrate and aggregate into clusters in the middle of enterable pores, which causes the re-exposure of oxygen- and sulfur-containing groups for gas adsorption.

Moisture has a bigger effect on the adsorption of CO_2 than that of CH_4, since both H_2O and CO_2 have high affinity with the oxygen- and sulfur-containing groups. A certain amount of moisture can potentially

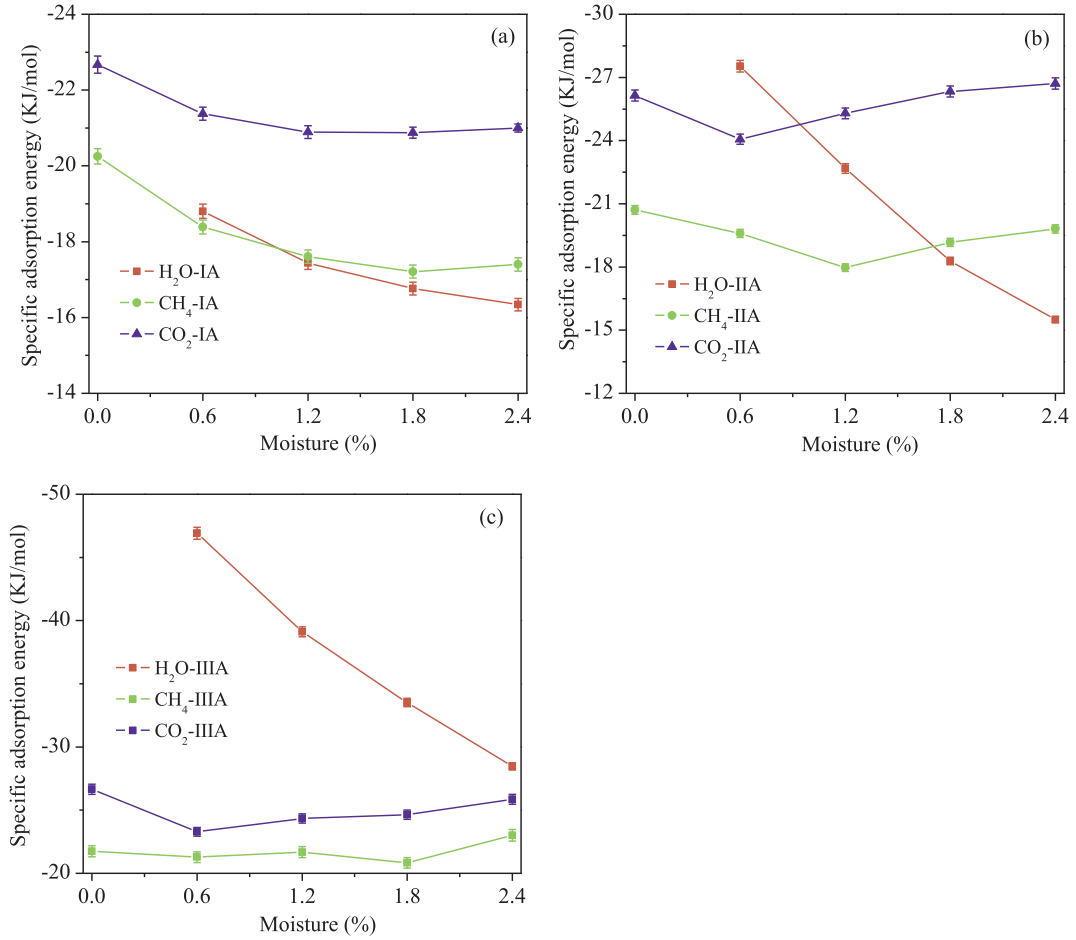

Fig. 15. Effect of moisture on the specific adsorption energy between $CH_4/CO_2/H_2O$ and kerogen systems at 30 MPa with $y_{CO_2} = 0.5$. (a) Kerogen IA model; (b) kerogen IIA model; (c) kerogen IIIA model.

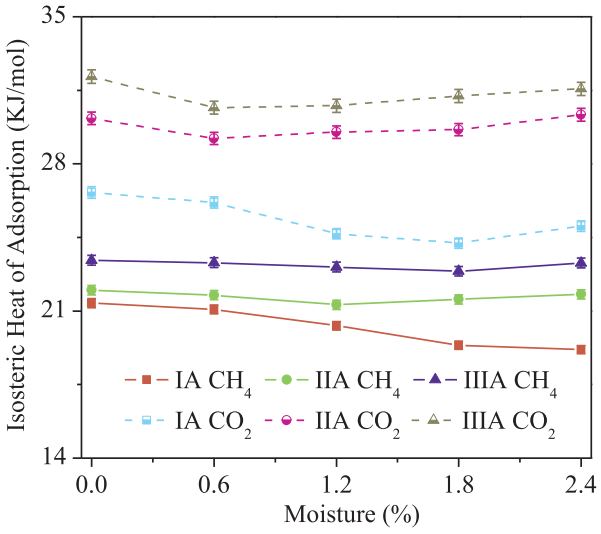

Fig. 16. Effect of moisture on the isosteric heat of CH_4 and CO_2 adsorption in the mixture at 30 MPa with $y_{CO_2} = 0.5$.

boost the displacement of CH_4 by CO_2, thus improving the efficiency of CS-EGR. The CH_4 and CO_2 adsorption capacity decrease with increasing moisture content, while the CO_2/CH_4 adsorption selectivity, specific adsorption energy and CO_2 isosteric heat decrease at the beginning, and then increase slowly with increasing moisture content. The early decrease can be attributed to the occupation of polar functional groups by H_2O molecules, while the later increase is related to the aggregation and migration of H_2O molecules, which re-exposures some polar functional groups occupied by H_2O molecules.

Acknowledgments

This work was supported by the National Natural Science Foundation of China (Grant No. 51774298 and 51504265) and the Science Foundation for the Excellent Youth Scholars of China University of Petroleum (Beijing) (Grant No. 2462015YQ0223). Computer time for this study was provided by the HP High Performance Computing Cluster of the State Key Laboratory of Heavy Oil Processing at China University of Petroleum (Beijing).

Notes

The authors declare no competing financial interest. Colors for illustrations are not required in the printed version.

References

[1] Paylor A. The social–economic impact of shale gas extraction: a global perspective. Third World Q 2017;38(2):340–55.
[2] Yuan J, Luo D, Feng L. A review of the technical and economic evaluation techniques for shale gas development. Appl Energy 2015;148:49–65.
[3] Weijermars R. US shale gas production outlook based on well roll-out rate scenarios. Appl Energy 2014;124:283–97.
[4] Yamazaki T, Aso K, Chinju J. Japanese potential of CO_2 sequestration in coal seams. Appl Energy 2006;83(9):911–20.
[5] Karacan CÖ, et al. Coal mine methane: a review of capture and utilization practices with benefits to mining safety and to greenhouse gas reduction. Int J Coal Geol 2011;86:121–56.
[6] Weijermars R. Economic appraisal of shale gas plays in Continental Europe. Appl Energy 2013;106:100–15.
[7] Huang Y et al. Optimal scheduling for enhanced coal bed methane production through CO2 injection 2014;113:1475–83.
[8] Kim TH, Cho J, Lee KS. Evaluation of CO_2 injection in shale gas reservoirs with multi-component transport and geomechanical effects. Appl Energy 2017;190:1195–206.
[9] White CM, et al. Sequestration of carbon dioxide in coal with enhanced coalbed methane recovery a review. Energ Fuel 2005;19(3):659–724.
[10] Chatterjee R, Paul S. Classification of coal seams for coal bed methane exploitation in central part of Jharia coalfield, India – a statistical approach. Fuel 2013;111:20–9.
[11] Vishal V, Singh TN, Ranjith PG. Influence of sorption time in CO_2-ECBM process in Indian coals using coupled numerical simulation. Fuel 2015;139:51–8.
[12] Jiang X. A review of physical modelling and numerical simulation of long-term geological storage of CO_2. Appl Energy 2011;88(11):3557–66.
[13] Middleton RS, et al. Shale gas and non-aqueous fracturing fluids: opportunities and challenges for supercritical CO_2. Appl Energy 2015;147:500–9.
[14] Eshkalak MO et al. Enhanced gas recovery by CO_2 sequestration versus re-fracturing treatment in unconventional shale gas reservoirs. In: Proceedings of the Abu Dhabi international petroleum exhibition and conference, Society of Petroleum Engineers, Abu Dhabi, UAE, Nov 10–13, 2014 SPE 172083; 2014.
[15] Huang L, et al. Thermodynamic and structural characterization of bulk organic matter in Chinese Silurian shale: experimental and molecular modeling studies. Energ Fuel 2017;31(5):4851–65.
[16] Curtis JB. Fractured shale-gas systems. Am Asso Petrol Geol Bull 2002;86(11):1921–38.
[17] Collell J, et al. Transport of multicomponent hydrocarbon mixtures in shale organic matter by molecular simulations. J Phys Chem C 2015;119(39):22587–95.
[18] Wu K, et al. Model for surface diffusion of adsorbed gas in nanopores of shale gas reservoirs. Ind Eng Chem Res 2015;54(12):3225–36.
[19] Wang F, Reed RM. Pore networks and fluid flow in gas shales. In: Proceedings of the SPE annual technical conference and exhibition, Society of Petroleum Engineers, New Orleans, LA, Oct 4 – 7, 2009. SPE 124253; 2009.
[20] Gasparik M, et al. Geological controls on the methane storage capacity in organic-rich shales. Int J Coal Geol 2014;123:34–51.
[21] Ross DJK, Bustin RM. The importance of shale composition and pore structure upon gas storage potential of shale gas reservoirs. Mar Petrol Geol 2009;26(6):916–27.
[22] Tissot B, et al. Influence of the nature and diagenesis of organic matter in formation of petroleum. Am Asso Petrol Geol Bull 1974;58(3):499–506.
[23] Ungerer P, Collell J, Yiannourakou M. Molecular modeling of the volumetric and thermodynamic properties of kerogen: influence of organic type and maturity. Energ Fuel 2014;29(1):91–105.
[24] Boult P, Theologou P, Foden J. Capillary seals within the Eromanga basin, Australia: implications for exploration and production. In: Surdam RC, editor. Seals, traps and the petroleum system. Am. Assoc. Pet. Geol. Memoir, vol. 67; 1997. p. 143–68.
[25] Gensterblum Y, et al. High-pressure CH_4 and CO_2 sorption isotherms as a function of coal maturity and the influence of moisture. Int J Coal Geol 2013;118:45–57.
[26] Hu Y, et al. Microscopic dynamics of water and hydrocarbon in shale-kerogen pores of potentially mixed wettability. SPE J 2014;20(01):112–24.
[27] Herrle JO, et al. Forcing mechanisms for mid-Cretaceous black shale formation: evidence from the Upper Aptian and Lower Albian of the Vocontian Basin (SE France). Palaeogeogr Palaeocl 2003;190:399–426.
[28] Krooss B, et al. High pressure methane and carbon dioxide adsorption on dry and moisture equilibrated Pennsylvanian coals. Int J Coal Geol 2002;51(2):69–92.
[29] Li J, et al. Water distribution characteristic and effect on methane adsorption capacity in shale clay. Int J Coal Geol 2016;159:135–54.
[30] Li J, et al. Water sorption and distribution characteristics in clay and shale: effect of surface force. Energ Fuel 2016;30(11):8863–74.
[31] Luo F, Xu RN, Jiang PX. Numerical investigation of the influence of vertical permeability heterogeneity in stratified formation and of injection/production well perforation placement on CO_2 geological storage with enhanced CH_4 recovery. Appl Energy 2013;102:1314–23.
[32] Yu W, Al-Shalabi EW, Sepehrnoori K. A sensitivity study of potential CO2 injection for enhanced gas recovery in Barnett shale reservoirs. In: Proceedings of the SPE unconventional resources conference. Society of Petroleum Engineers, Woodlands, Texas, April 1–3, SPE 169012; 2014.
[33] Jiang J, Shao Y, Younis RM. Development of a multi-continuum multicomponent model for enhanced gas recovery and CO2 storage in fractured shale gas reservoirs. In: Proceedings of the SPE improved oil recovery symposium. Society of Petroleum Engineers, Tulsa, Oklahoma, April 12–16, 2014. SPE 169114; 2014.
[34] Godec M, et al. Potential for enhanced gas recovery and CO_2 storage in the Marcellus shale in the Eastern United States. Int J Coal Geol 2013;118:95–104.
[35] Liu F, et al. Assessing the feasibility of CO_2 storage in the New Albany Shale (Devonian-Mississippian) with potential enhanced gas recovery using reservoir simulation. Int J Greenhouse Gas Control 2013;17:111–26.
[36] Gensterblum Y, Busch A, Krooss BM. Molecular concept and experimental evidence of competitive adsorption of H_2O, CO_2 and CH_4 on organic material. Fuel 2014;115:581–8.
[37] Ottiger S, et al. Measuring and modeling the competitive adsorption of CO_2, CH_4, and N_2 on a dry coal. Langmuir 2008;24(17):9531–40.
[38] Bhowmik S, Dutta P. Investigation into the methane displacement behavior by cyclic, pure carbon dioxide injection in dry, powdered, bituminous Indian coals. Energ Fuel 2011;25(6):2730–40.
[39] Faiz MM, et al. Evaluating geological sequestration of CO_2 in bituminous coals: the southern Sydney Basin, Australia as a natural analogue. Int J Greenhouse Gas Control 2007;1(2):223–35.
[40] Khosrokhavar R, Wolf KH, Bruining H. Sorption of CH_4 and CO_2 on a carboniferous shale from Belgium using a manometric setup. Int J Coal Geol 2014;128:153–61.
[41] Busch A, Gensterblum Y, Krooss BM. Methane and CO_2 sorption and desorption measurements on dry Argonne premium coals: pure components and mixtures. Int J Coal Geol 2003;55(2):205–24.
[42] Majewska Z, et al. Binary gas sorption/desorption experiments on a bituminous coal: simultaneous measurements on sorption kinetics, volumetric strain and acoustic emission. Int J Coal Geol 2009;77(1):90–102.
[43] Ross DJ, Bustin RM. Impact of mass balance calculations on adsorption capacities in

microporous shale gas reservoirs. Fuel 2007;86(17):2696–706.
[44] Zhang J, et al. Molecular simulation of CO_2–CH_4 competitive adsorption and induced coal swelling. Fuel 2015;160:309–17.
[45] Kazemi M, Takbiri-Borujeni A. Molecular dynamics study of carbon dioxide storage in carbon-based organic nanopores. SPE181705; 2016.
[46] Kurniawan Y, Bhatia SK, Rudolph V. Simulation of binary mixture adsorption of methane and CO_2 at supercritical conditions in carbons. AIChE J 2006;52(3):957–67.
[47] Yuan Q, et al. Molecular dynamics simulations of the enhanced recovery of confined methane with carbon dioxide. Phys Chem Chem Phys 2015;17:31887–93.
[48] Brochard L, et al. Adsorption-induced deformation of microporous materials: coal swelling induced by CO_2-CH_4 competitive adsorption. Langmuir 2012;28:2659–70.
[49] Wang X, et al. Molecular simulation of CO_2/CH_4 competitive adsorption in organic matter pores in shale under certain geological conditions. Petrol Explor Dev 2016;43(5):841–8.
[50] Lu X, et al. Competitive adsorption of a binary CO_2-CH_4 mixture in nanoporous carbons: effects of edge-functionalization. Nanoscale 2015;7(3):1002–12.
[51] Liu X, et al. Molecular simulation of CH_4, CO_2, H_2O and N_2 molecules adsorption on heterogeneous surface models of coal. Appl Surf Sci 2016;389:894–905.
[52] Sun H, et al. Molecular insights into the enhanced shale gas recovery by carbon dioxide in kerogen slit nanopores. J Phys Chem C 2017;121(18):10233–41.
[53] Huang L, et al. Molecular simulation of adsorption behaviors of methane, carbon dioxide and their mixtures on kerogen: effect of kerogen maturity and moisture content. Fuel 2018;211:159–72.
[54] Kelemen SR, et al. Direct Characterization of Kerogen by X-ray and Solid-State ^{13}C Nuclear Magnetic Resonance Methods. Energ Fuel 2007;21(3):1548–61.
[55] Materials Studio. A material modeling software of Accelrys Company, United States; 2012. < www.accelrys.com > .
[56] Sun H. COMPASS: an ab initio force-field optimized for condensed phase applications overview with details on alkane and benzene compounds. J Phys Chem B 1998;102(38):7338–64.
[57] Sui H, Yao J. Effect of surface chemistry for CH_4/CO_2 adsorption in kerogen: a molecular simulation study. J Nat Gas Sci Eng 2016;31:738–46.
[58] Ru X, et al. Experimental and computational studies on the average molecular structure of Chinese Huadian oil shale kerogen. J Mol Struct 2012;1030:10–8.
[59] Zhao T, et al. Molecular simulation of adsorption and thermodynamic properties on type II kerogen: influence of maturity and moisture content. Fuel 2017;190:198–207.
[60] Collell J, et al. Molecular simulation of bulk organic matter in Type II shales in the middle of the oil formation window. Energ Fuel 2014;28(12):7457–66.
[61] Gasparik M, et al. “Multi-temperature” method for high-pressure sorption measurements on moist shales. Rev Sci Instrum 2013;84(8):085116.
[62] Zhang J, et al. Combined Monte Carlo and molecular dynamics simulation of methane adsorption on dry and moist coal. Fuel 2014;122:186–97.
[63] Wang W, et al. Carbon dioxide adsorption thermodynamics and mechanisms on MCM-41 supported polyethylenimine prepared by wet impregnation method. Appl Energy 2015;142:221–8.
[64] Mathias PM, Copeman TW. Extension of the Peng-Robinson equation of state to complex mixtures: evaluation of the various forms of the local composition concept. Fluid Phase Equilibr 1983;13:91–108.
[65] Connolly ML. Solvent-accessible surfaces of proteins and nucleic acids. Science 1983;221(4612):709–13.
[66] Pan H, Ritter JA, Balbuena PB. Examination of the approximations used in determining the isosteric heat of adsorption from the Clausius-Clapeyron equation. Langmuir 1998;14(21):6323–7.
[67] Facelli JC, Pugmire R, Pimienta I. Atomistic modeling of oil shale kerogens and asphaltenes along with their interactions with the inorganic mineral matrix. Salt Lake City, UT: University of Utah; 2011.
[68] Mastalerz M, et al. Influence of maceral composition on geochemical characteristics of immature shale kerogen: insight from density fraction analysis. Int J Coal Geol 2012;103:60–9.
[69] Rexer TF, et al. High-pressure methane adsorption and characterization of pores in Posidonia shales and isolated kerogens. Energ Fuel 2014;28(5):2886–901.
[70] Loucks RG, et al. Morphology, genesis and distribution of nanometer-scale pores in siliceous mudstones of the Mississippian Barnett Shale. J Sediment Res 2009;79(12):848–61.
[71] Zhang T, et al. Effect of organic-matter type and thermal maturity on methane adsorption in shale-gas systems. Org Geochem 2012;47:120–31.
[72] Gasparik M, et al. First international inter-laboratory comparison of high-pressure CH_4, CO_2 and C_2H_6 sorption isotherms on carbonaceous shales. Int J Coal Geol 2014;132:131–46.
[73] Bae JS, Nguyen TX, Bhatia SK. Pore accessibility of Ti_3SiC_2-derived carbons. Carbon 2014;68:531–41.
[74] Bae JS, et al. Pore accessibility of methane and carbon dioxide in coals. Energ Fuel 2009;23(6):3319–27.
[75] Bae JS, Bhatia SK. High-pressure adsorption of methane and carbon dioxide on coal. Energ Fuel 2006;20(6):2599–607.
[76] Nguyen TX, Bhatia SK. Determination of pore accessibility in disordered nanoporous materials. J Phys Chem C 2007;111(5):2212–22.
[77] Nguyen TX, Bhatia SK. Kinetic restriction of simple gases in porous carbons: transition-state theory study. Langmuir 2008;24(1):146–54.
[78] Gregg SJ, Sing KS. adsorption, surface area and porosity. New York: Academic Press; 1982. p. 4.
[79] Xiong J, et al. Adsorption of methane in organic-rich shale nanopores: an experimental and molecular simulation study. Fuel 2017;200:299–315.
[80] Dang Y, et al. Molecular simulation of CO_2/CH_4 adsorption in brown coal: effect of oxygen-, nitrogen-, and sulfur-containing functional groups. Appl Surf Sci 2017;423:33–42.
[81] Weniger P, et al. Investigations on the methane and carbon dioxide sorption capacity of coals from the SW Upper Silesian Coal Basin, Czech Republic. Int J Coal Geol 2012;93:23–39.
[82] Bachu S. Sequestration of CO_2 in geological media in response to climate change: road map for site selection using the transform of the geological space into the CO_2 phase space. Energy Convers Manage 2002;43(1):87–102.